

Simultaneous Search for Extra Light and Heavy Higgs Bosons via Cascade Decays

Ulrich Ellwanger^a and Matías Rodríguez-Vázquez^a

^a *Laboratoire de Physique Théorique, UMR 8627, CNRS, Université de Paris-Sud,
Université Paris-Saclay, 91405 Orsay, France*

Abstract

Models with extended Higgs sectors can contain several additional Higgs states, heavier or lighter than the SM Higgs boson. The couplings of lighter extra states to SM particles can be strongly reduced, leading to small cross sections for their direct production. Heavier extra states can have larger couplings to SM particles and, moreover, have large branching fractions into lighter extra states, notably into a SM-like Higgs boson accompanied by another Higgs state which can be lighter or heavier than 125 GeV. Motivated by corresponding scenarios in the NMSSM we study the prospects for the discovery or exclusion of cascade decays $ggF \rightarrow H_3 \rightarrow H_2 + H_1$ in the $b\bar{b}b\bar{b}$, $b\bar{b}\tau\tau$ and $b\bar{b}\gamma\gamma$ final states where either H_1 or H_2 can be SM-like. Significant regions of the NMSSM parameter space can be tested by these searches. These are, however, not confined to models of the NMSSM type.

1 Introduction

Extended Higgs sectors are frequent properties of models beyond the Standard Model (BSM). Such extra states can have very small couplings to quarks, leptons and SM gauge fields. For instance, for singlets under the SM gauge symmetries such renormalizable couplings are disallowed by gauge invariance. The direct production cross sections for these states are then strongly suppressed in all channels. On the other hand, couplings of singlets to SU(2) Higgs doublets of the SM- or BSM-type are possible and typically present in BSM models. This allows for the discovery of such states in cascade decays of heavy BSM SU(2) Higgs doublets, provided the production cross sections of the latter are large enough.

The final states after BSM-Higgs to BSM-Higgs + SM-Higgs cascades typically correspond to the ones in searches for resonant SM-Higgs (H_{125}) pair production: mainly $b\bar{b}b\bar{b}$, $b\bar{b}\tau\tau$ and $b\bar{b}\gamma\gamma$. Corresponding searches have been performed at the LHC by ATLAS [1–6] and by CMS [7–21]. However, one of the SM-like Higgs bosons would now be replaced by a lighter or heavier BSM-Higgs boson. One can argue that the cross sections for such processes can be more promising than for resonant SM-Higgs pair production:

- a) A sizeable gluon-gluon-fusion (ggF) production cross section of a heavy scalar or pseudoscalar Φ , i.e. a sizeable coupling of Φ to top quarks, requires Φ to possess a sizeable SU(2)-doublet component. However, since H_{125} is also a SU(2)-doublet, trilinear couplings $\Phi - H_{125} - H_{125}$ (with Φ a pure doublet) violate the SU(2) symmetry and must be proportional to a SU(2) symmetry breaking vev; the latter is limited from above by the Z/W masses. This limits the possible partial width for $\Phi \rightarrow H_{125} + H_{125}$, whereas the concurrent decay $\Phi \rightarrow t\bar{t}$ is always possible if Φ can be produced in ggF and is heavier than $2m_{top}$.
- b) In the case $ggF \rightarrow \Phi \rightarrow H_{125} + H'$ with Φ a pure doublet, the trilinear coupling $\Phi - H_{125} - H'$ can be SU(2) invariant if H' is a singlet. In models with extended Higgs sectors including both an extra doublet and a singlet, such a coupling can thus be much larger than the Z/W masses leading to sizeable $\Phi \rightarrow H_{125} + H'$ partial widths.

In Two-Higgs-Doublet-Models of type II such as the Minimal Supersymmetric Standard Model (MSSM) the production cross sections for extra CP-even (H) and CP-odd (A) Higgs doublets are not suppressed, and are dominated by ggF for $\tan\beta$ not too large [22–24]. H or A can thus play the rôle of Φ above. The Next-to-Minimal Supersymmetric Standard Model (NMSSM) [25, 26] contains additional CP-even (H_S) and CP-odd (A_S) singlet-like states with masses typically below $M_H \sim M_A$. One finds that the $BR(H \rightarrow H_S + H_{125})$ and $BR(A \rightarrow A_S + H_{125})$ can be up to $\sim 50\%$ [27–32], for the reasons given above and detailed in the next section.

In the NMSSM this offers the possibility to produce otherwise practically invisible mostly singlet-like states H_S/A_S in cascade decays of H/A [27–32]. It is the aim of the present paper to study the prospects for discovery or exclusion of, simultaneously, H/A and H_S/A_S states in $ggF \rightarrow H \rightarrow H_S + H_{125}$ or $ggF \rightarrow A \rightarrow A_S + H_{125}$ in the final states $b\bar{b}b\bar{b}$, $b\bar{b}\tau\tau$ and $b\bar{b}\gamma\gamma$. Supersymmetry plays no rôle here, accordingly our results are applicable to any models with similarly extended Higgs sectors; see, e.g., [33].

We will adopt various strategies from the searches for resonant SM Higgs pair production by ATLAS [1–6] and by CMS [7–21]. Moreover, for M_{H_S} near 125 GeV we can compare our backgrounds and expected 95% CL upper limits on the cross sections times branching

fractions to the ones obtained in these publications.

On the other hand, the analyses presented here are complicated by the fact that the masses M_{H_S}/M_{A_S} are not known *a priori*. An important aspect of optimal search strategies are M_{H_S}/M_{A_S} dependent selection criteria (cuts) on events, hence different analyses should be performed, varying the assumptions on M_{H_S}/M_{A_S} . Only at the end of each of these analyses a search for a resonance-like bump in the total invariant mass of the H_S/A_S plus H_{125} decay products, which should correspond to M_H/M_A , is proposed.

In the next section we discuss shortly the Higgs sector of the NMSSM and the couplings relevant for the processes considered here. In section 3 we present features of our signal simulations. In section 4 we discuss the optimal search strategy for the $b\bar{b}b\bar{b}$ final state, and compare expected 95% CL upper limits and 5σ discovery limits on the cross sections times branching fractions to the ones possible in the NMSSM. Sections 5 and 6 are devoted to the $b\bar{b}\tau\tau$ and $b\bar{b}\gamma\gamma$ final states. All these search strategies and results are identical for $ggF \rightarrow H \rightarrow H_S + H_{125}$ and $ggF \rightarrow A \rightarrow A_S + H_{125}$, for notational simplicity we will refer to $H \rightarrow H_S + H_{125}$ only. In section 7 we conclude with a summary and an outlook.

2 The neutral Higgs sector of the NMSSM

In this section we discuss briefly some properties of the Higgs sector of the CP-conserving \mathbb{Z}_3 -invariant NMSSM. It consists in two SU(2) doublets H_u , H_d and a complex singlet S . The superpotential of the Higgs sector reads

$$W_{\text{Higgs}} = \lambda \hat{S} \hat{H}_u \cdot \hat{H}_d + \frac{\kappa^3}{3} \hat{S}^3 \quad (2.1)$$

where λ and κ are dimensionless Yukawa couplings, and \hat{H}_u , \hat{H}_d and \hat{S} denote chiral superfields. Once the real component of the superfield \hat{S} develops a vacuum expectation value (vev) s , the first term in the superpotential generates an effective μ term

$$\mu = \lambda s. \quad (2.2)$$

The vev v_u of H_u generates up-type quark masses, the vev v_d of H_d generates masses for down-type quarks and leptons, and both vevs contribute to the Z and W^\pm masses. Their ratio is $\tan\beta = v_u/v_d$.

Decays of a heavy Higgs state into two lighter Higgs states occur in the presence of corresponding trilinear Higgs couplings. Most of the trilinear Higgs couplings in the \mathbb{Z}_3 -invariant NMSSM originate from quartic terms in the Higgs potential (see [25, 26]) proportional to two powers of λ , κ or the electroweak gauge couplings, once the (neutral) Higgs fields are expanded around their vevs and decomposed into their real and imaginary parts:

$$H_u^0 = v_u + \frac{1}{\sqrt{2}}(H_{u,r}^0 + iH_{u,i}^0), \quad H_d^0 = v_d + \frac{1}{\sqrt{2}}(H_{d,r}^0 + iH_{d,i}^0), \quad S = s + \frac{1}{\sqrt{2}}(S_r + iS_i). \quad (2.3)$$

Hence the trilinear couplings are proportional to the vevs v_u , v_d or s . Whereas v_u , v_d are limited from above by $M_Z^2 = \frac{g_1^2 + g_2^2}{2}(v_u^2 + v_d^2)$, a large vev s can generate a trilinear coupling

$\sim H_u \cdot H_d S$. Another source for such a coupling is a trilinear Higgs-dependent soft SUSY breaking term

$$\lambda A_\lambda H_u \cdot H_d S + h.c. \quad (2.4)$$

where the dimensionful parameter A_λ can be much larger than Higgs vevs.

In order to obtain its impact on trilinear couplings among Higgs mass eigenstates, the mass matrices have to be diagonalized. In the CP-even sector, where one deals with a 3×3 mass matrix, a first step in this direction is a rotation in the SU(2) doublet sector into the so-called Higgs basis

$$H_{u,r}^0 = \sin \beta h' - \cos \beta H', \quad H_{d,r}^0 = \cos \beta h' + \sin \beta H' \quad (2.5)$$

where the vev of H' is zero, and the vev $\langle h' \rangle = \sqrt{v_u^2 + v_d^2}$ is equal to the one of the SM Higgs boson. In fact, in most of the phenomenological acceptable regions of the parameter space of the NMSSM (near the alignment limit [29]) the eigenstates of the full 3×3 CP-even mass matrix are not very different from h' , H' and S_r , and will be denoted by H_{125} ($\sim h'$, approximately SM-like), H ($\sim H'$, approximately MSSM-like) and H_S ($\sim S_r$, approximately singlet-like) in the following.

The corresponding rotation of the imaginary components $H_{u,i}^0$ and $H_{d,i}^0$ (with $\beta \rightarrow -\beta$) diagonalizes their 2×2 mass submatrix exactly and generates the Goldstone boson together with the MSSM-like pseudoscalar A' . The latter still mixes with the singlet-like S_i , but typically both differ little from the mass eigenstates A and A_S .

Performing the rotation (2.5) in (2.4) and using the previous approximations in the CP-even and CP-odd sectors, one obtains the trilinear couplings

$$\frac{\lambda A_\lambda}{\sqrt{2}} \left(\frac{\tan^2 \beta - 1}{\tan^2 \beta + 1} H_{125} (HH_S - AA_S) + \dots \right) \quad (2.6)$$

where the omitted terms are suppressed by $\tan \beta$. Hence, for not too small $\tan \beta \rightarrow 1$, trilinear couplings $g_{H_{125}HH_S}$ and $g_{H_{125}AA_S}$ are generated which have no analog in the MSSM, and are larger than all other trilinear Higgs couplings if λA_λ is large.

On the other hand the masses $M_{H/A}$ of the nearly degenerate mostly MSSM-like states H/A are approximatively given by

$$M_{H/A}^2 \sim \mu \left(A_\lambda + \frac{\kappa}{\lambda} \mu \right) \frac{1 + \tan^2 \beta}{\tan \beta}, \quad (2.7)$$

which limits A_λ from above for fixed $M_{H/A}$, $\tan \beta$, small $|\kappa/\lambda|$ and $|\mu| \gtrsim 100$ GeV (as required by the lower LEP bound on higgsino-like charginos). Accordingly the trilinear couplings $g_{H_{125}HH_S}$ and $g_{H_{125}AA_S}$ can be larger for larger $M_{H/A}^2$.

The production cross sections for the mostly MSSM-like states H/A is dominated by ggF [22–24]; at $\sqrt{s} = 13 - 14$ TeV and for $\tan \beta \sim 2 - 3$ (typical in the NMSSM) they are $\gtrsim \mathcal{O}(1 \text{ pb})$ up to $M_{H/A} \sim 600$ GeV. The trilinear couplings $g_{H_{125}HH_S}$ and $g_{H_{125}AA_S}$ induce the decays $H \rightarrow H_{125} + H_S$ and $A \rightarrow H_{125} + A_S$ if kinematically allowed. The branching fractions $BR(H/A \rightarrow H_{125} + H_S/A_S)$ can be as large as $\sim 50\%$, in contrast to the decay $H \rightarrow H_{125} + H_{125}$.

The singlet-like states $\Phi_S = H_S/A_S$ have small couplings to quarks, leptons and gauge fields induced by mixings with h' , H' and A' . Hence the production cross sections for Φ_S are typically small, and their discovery may have to rely on $H/A \rightarrow H_{125} + \Phi_S$ decays. Via the couplings induced by mixing, Φ_S can decay into the same channels as H_{125} and H/A . For $M_{\Phi_S} > 2m_{top}$, decays into $t\bar{t}$ are dominant, whereas decays $\Phi_S \rightarrow b\bar{b}$ dominate typically for $M_{\Phi_S} < 2m_{top}$. (The branching ratio for $H_S \rightarrow W^+W^-$ can also be sizeable [29].) For $M_{H_S} > 250$ GeV, decays $H_S \rightarrow H_{125} + H_{125}$ are possible, leading to double-resonant tri-Higgs production (not considered here). Decays $\Phi_S \rightarrow \tau^+ + \tau^-$ are practically always possible. In the regions in the NMSSM parameter space with all present constraints on the signal rates of H_{125} being satisfied the $BR(\Phi_S \rightarrow \gamma + \gamma)$ is in the 0.1 – 0.3% range, making this decay observable as well. Henceforth we will consider resonant $b\bar{b}b\bar{b}$, $b\bar{b}\tau^+\tau^-$ and $b\bar{b}\gamma\gamma$ final states originating from $\Phi_S \rightarrow b\bar{b}$, $\Phi_S \rightarrow \tau^+\tau^-$ and $\Phi_S \rightarrow \gamma\gamma$ decays.

Of interest will be the product of cross sections times branching fractions $\sigma(ggF \rightarrow H/A) \times BR(H/A \rightarrow H_{125} + H_S/A_S \rightarrow b\bar{b}b\bar{b}, b\bar{b}\tau^+\tau^- \text{ and } b\bar{b}\gamma\gamma)$ for various masses M_H , M_{H_S} and M_{A_S} , for realistic regions in the parameter space of the NMSSM. To this end we have performed scans using the public code `NMSSMTools_5.1.0` [34, 35] including the radiative corrections from [36]. All phenomenological constraints, including the absence of Landau singularities below the GUT scale and, notably, constraints from Higgs searches in various channels at LEP and LHC are applied.

These include searches for scalar and pseudoscalar Higgs production at LEP (including unconventional Higgs decays), constraints from B -physics, constraints on the mass of H_{125} (± 3 GeV to account for theoretical uncertainties) and on its signal rates from the combined ATLAS and CMS run I results which disallow too large $H_{125} - H_S$ mixings, constraints from searches for $ggF \rightarrow H_S \rightarrow \gamma\gamma$ for $M_{H_S} = 65 - 122$ GeV, and searches for H/A in the $H/A \rightarrow \tau\tau$ channel with H/A produced in association with b -quarks and via ggF . We note that constraints from these latter searches in the $M_A - \tan\beta$ plane are weak for $\tan\beta \approx 2 - 3$, typical in the NMSSM, and further alleviated if H/A have large branching fractions into the final states considered here.

The results of these scans for $\sigma(ggF \rightarrow H/A) \times BR(H/A \rightarrow H_{125} + H_S/A_S \rightarrow b\bar{b}b\bar{b}, b\bar{b}\tau^+\tau^- \text{ and } b\bar{b}\gamma\gamma)$ will be compared to the sensitivities in different final states in the following sections. The ggF production cross sections for H/A have been obtained from the CERN Yellow Report web page [37] at NNLO+NNLL, after an appropriate rescaling of the H/A -gluon-gluon coupling provided by `NMSSMTools_5.1.0`. Also the branching ratios of H/A and H_S/A_S are taken from `NMSSMTools_5.1.0`. In the Figures showing the 95% CL exclusion limits and 5σ discovery cross sections, viable values for the cross sections times branching fractions in the parameter space of the NMSSM will be indicated as light shaded blue regions for $ggF \rightarrow H \rightarrow H_{125} + H_S$, and as light shaded red regions for $ggF \rightarrow A \rightarrow H_{125} + A_S$. For simplicity we will use the notation $ggF \rightarrow H \rightarrow H_{125} + H_S$ for the search strategies; the same search strategies apply to $ggF \rightarrow A \rightarrow H_{125} + A_S$.

3 Simulation of Signal Samples

Signal events for the production of H in ggF are generated by `MadGraph5_aMC@NLO` [38] with matrix elements at NLO taken from `aMC_SusHi` [39–41] using the NNPDF2.3NLO PDF set [42] in the 4-flavour scheme. Renormalization and factorization scales are chosen as $H_T/2$ on an event-wise basis. `Pythia6.4` [43] is used for the $H \rightarrow H_{125} + H_S$ decays, the H_{125} and H_S decays and the subsequent showering and hadronization. The total widths of H are below $M_H/50$ in all cases, below $M_H/100$ for $M_H < 500$ GeV, hence the narrow width approximation is well satisfied.

Separate signal events have been generated for each pair (M_H, M_{H_S}) . For M_H we chose $M_H = 425, 500, 625, 750$ and 1000 GeV. We varied M_{H_S} in steps of 10 GeV in the range $25 - 225$ GeV, and in steps of 20 GeV above 225 GeV up to the kinematic boundary $M_H - 125$ GeV (except for $M_H = 1000$ GeV where M_{H_S} was varied in steps of 25/50 GeV).

For each pair (M_H, M_{H_S}) we generated 150k unweighted events, more than the expected number of events at 3000 fb^{-1} . Accordingly the statistical fluctuations from the Monte Carlo (MC) generation are small compared to the expected statistical fluctuations from the data; the latter will be taken into account.

The output is given to the detector simulation `Delphes 3` [44]. Jets are clustered with `FastJet 3.0.1` [45] using the anti- k_T algorithm with $\Delta R = 0.4$. For b -tagging the ATLAS card is used in `Delphes 3`.

The p_T dependence of the b -tagging and mistagging efficiencies is chosen in the ATLAS card following the parametrizations given in [46]. The default value of the parameters in `Delphes 3.3.2` correspond to a working point $\varepsilon_b = 70\%$ as, e.g., in the ATLAS search for Higgs pair production in the $4b$ final state at 13 TeV in [6]. We will employ the same settings except for the $b\bar{b}\gamma\gamma$ final state.

4 Search Strategy for the $b\bar{b}b\bar{b}$ Final State

Searches for resonant SM Higgs pair production in the $b\bar{b}b\bar{b}$ final state have been performed before by ATLAS at 8 TeV [1, 3, 4] and at 13 TeV [6], and by CMS at 8 TeV [8, 10, 12] and at 13 TeV [14, 15].

Searches for $ggF \rightarrow H \rightarrow H_S + H_{125} \rightarrow b\bar{b}b\bar{b}$ are complicated by the presence of two unknown masses of H and H_S . A naive approach would be to require one $b\bar{b}$ pair with a mass near 125 GeV, and to look for simultaneous excesses in the plane of invariant masses of the other $b\bar{b}$ pair and the total $4b$ invariant mass. However, this approach does not allow to optimize cuts as function of different masses of H and H_S . An at least $\sim 20\%$ gain in efficiency can be obtained as follows:

- a) Choose a tentative value for M_{H_S} , and optimise the cuts and the choice of $b\bar{b}$ pairs as function of this value;
- b) Search subsequently for an excess in the total $4b$ invariant mass (suitably corrected, see below).

Subsequently we describe first our simulation of signal samples and the strategies for the analysis. In the following subsections we discuss the background simulation and validation,

and finally the results for the expected 95% CL upper limits and 5σ discovery limits on the cross sections times branching fractions as function of M_H and M_{H_S} . The latter are compared to possible production cross sections times branching fractions in the NMSSM.

4.1 Analyses of Signal Samples

After the simulation of signal samples as described in section 3, at least four b -tagged jets with $p_T > 30$ GeV and $|\eta| < 2.5$ are required. Four b -tagged jets can be paired in six different ways. The two invariant masses of two $b\bar{b}$ pairs are tentatively denoted by $M_{b\bar{b}}(H_{125})$ and $M_{b\bar{b}}(H_S)$. The subsequent procedure depends on the chosen value for M_{H_S} , and has to be repeated for each choice.

An event is kept only if a pairing exists for which $M_{b\bar{b}}(H_{125})$ is sufficiently close to 125 GeV, and $M_{b\bar{b}}(H_S)$ is sufficiently close to M_{H_S} . In practice, the measured invariant masses of $b\bar{b}$ pairs are often somewhat smaller than the mass of the decaying Higgs boson. Therefore “sufficiently close to” should better be replaced by “slightly below” as in [6, 14]. Generalizing the conditions applied in [6, 14], an event is kept only if a pairing exists for which

$$\chi = \sqrt{\left(\frac{M_{b\bar{b}}(H_{125}) - 115 \text{ GeV}}{0.1 M_{b\bar{b}}(H_{125})}\right)^2 + \left(\frac{M_{b\bar{b}}(H_S) - 0.85 M_{H_S}}{0.1 M_{b\bar{b}}(H_S)}\right)^2} < 2. \quad (4.1)$$

If different pairings within a given event satisfy (4.1), the combination that minimizes χ is chosen. In Figs. 1 we show, for $M_H = 500$ GeV, the distributions of the dijet masses $M_{b\bar{b}}(H_{125})$ and $M_{b\bar{b}}(H_S)$ for the pairing minimizing χ , for two different benchmark points $M_{H_S} = 85$ GeV and $M_{H_S} = 340$ GeV in the case where M_{H_S} for the analysis was chosen correctly. The black contours indicate the signal regions defined by $\chi < 2$.¹

In the case of heavy resonances with masses above ~ 1 TeV, the two b -jets from a single Higgs boson tend to merge into a single fat jet. Accordingly a “boosted” analysis based on single $\Delta R = 1.0$ jets per Higgs boson was applied in [6] for searches for such heavy resonances. We found that for such heavy H states the production cross sections become too small for reasonable sensitivities, and limit ourselves to $M_H \leq 1$ TeV subsequently. We had tried to vary the jet reconstruction parameter ΔR without observing, however, a major impact on the possible sensitivities. The next step in the event selection are cuts on p_T of the $b\bar{b}$ pairs associated with H_{125} and H_S , respectively.

These cuts can be optimised with respect to M_{4b} (defined by the event) and the tentative value for M_{H_S} . To this end we considered many samples of $M_H \sim M_{4b}$ and M_{H_S} . In each case we studied the dependence of the sensitivity $\epsilon_s/\sqrt{\epsilon_B}$ (ϵ_s and ϵ_B denote the efficiencies of the signal and background, respectively) on the cuts on p_T . Maximizing the sensitivities, we obtain different values for the optimal cuts on p_T for each sample of M_{4b} and M_{H_S} . These different values for the cuts on p_T are well approximated by the following functions of M_{4b}

¹An alternative pairing algorithm based on the angular distances of the constituent b -jets was studied. We found that the resulting sensitivities are mostly similar to those obtained using the mass-based algorithm described above when the jets are sufficiently collimated. However, as M_{H_S} increases, the jets become too back-to-back, making the angular-pairing contraproductive. For this reason, we used the mass-based algorithm for the reconstruction of the Higgs candidates.

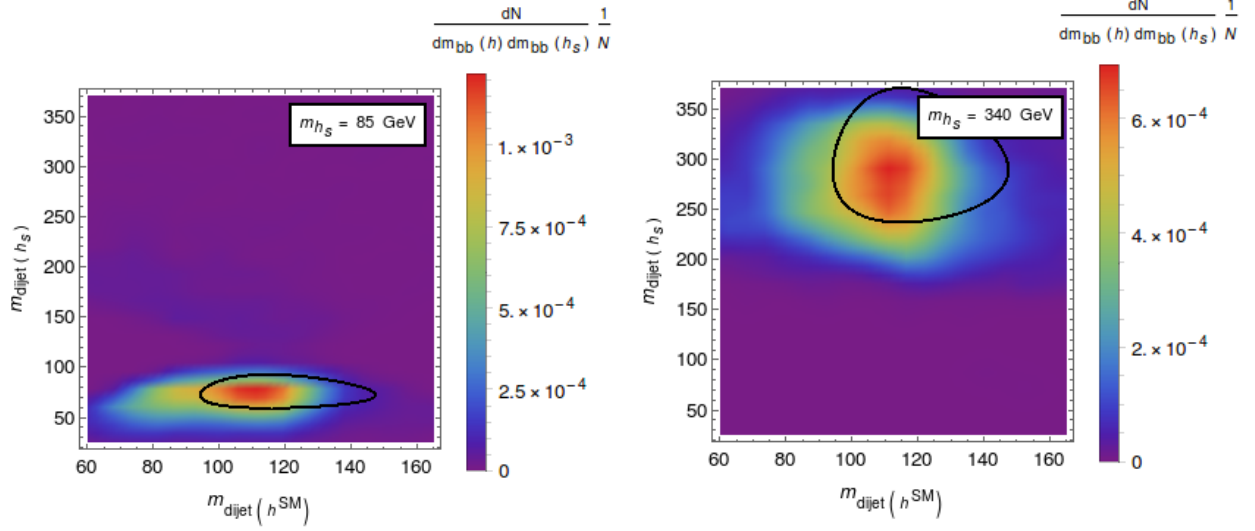


Figure 1: Dijet mass distributions $M_{b\bar{b}}(H_{125})$ and $M_{b\bar{b}}(H_S)$ for two different benchmark points $M_{H_S} = 85$ GeV and $M_{H_S} = 340$ GeV. The black contours indicate the signal regions defined by $\chi < 2$.

and M_{H_S} :

$$\begin{aligned}
 p_T(b\bar{b}(H_{125})) &> 1.6 \text{ GeV} + 0.4 M_{4b} - 0.13 M_{H_S} - \frac{M_{H_S}}{M_{4b}} \cdot 160 \text{ GeV} \\
 p_T(b\bar{b}(H_S)) &> 12 \text{ GeV} + 0.4 M_{4b} - 0.15 M_{H_S} - \frac{M_{H_S}}{M_{4b}} \cdot 166 \text{ GeV}
 \end{aligned} \tag{4.2}$$

The efficiencies of the three cuts a) $4b$ with $p_T > 30$ GeV, b) signal region (4.1) and c) dijet p_T (4.2) are shown in Figs. 2 for $M_{H_S} = 75$ GeV and $M_{H_S} = 325$ GeV as function of M_H , and in Figs. 3 for $M_H = 625$ GeV and $M_H = 1000$ GeV as function of M_{H_S} . One observes a decrease of the efficiency of the condition of four b -tagged jets for $M_{H_S} \lesssim 80$ GeV (for $M_H = 625$ GeV) and $M_{H_S} \lesssim 100$ GeV (for $M_H = 1000$ GeV). Here the two b -jets from H_S are boosted and hardly get resolved by the standard jet clustering algorithm; dedicated boosted analyses as in [6] could be invoked for this configuration.

For the search for a resonance H we found it useful to replace M_{4b} by M_X , with M_X defined such that uncertainties in the measurements of $M_{b\bar{b}}$ relative to $M_{H_{125}}$ and M_{H_S} (typically due to radiation out of the jet cones) are corrected:

$$M_X = M_{4b} + 125 \text{ GeV} - M_{b\bar{b}}(H_{125}) + M_{H_S} - M_{b\bar{b}}(H_S). \tag{4.3}$$

The empirical variable M_X was already used by CMS in resonant double Higgs production search in the $b\bar{b}\gamma\gamma$ channel [14]. We found that replacing M_X by a full Lorentz covariant expression in terms of $M_{H_{125}}$, M_{H_S} and the two values of $M_{b\bar{b}}$ did not improve the sensitivities.

In Fig. 4 we show the distributions of the reconstructed masses M_{4b} and M_X for the signal samples $(M_H, M_{H_S}) = (350, 195), (500, 310), (750, 450), (1000, 600)$ GeV. We clearly see a sharpening of the peaks using M_X in each case.

In order to obtain the required production cross sections times branching fractions for 5σ discovery or 95% CL exclusion we have to obtain the background distribution of M_X .

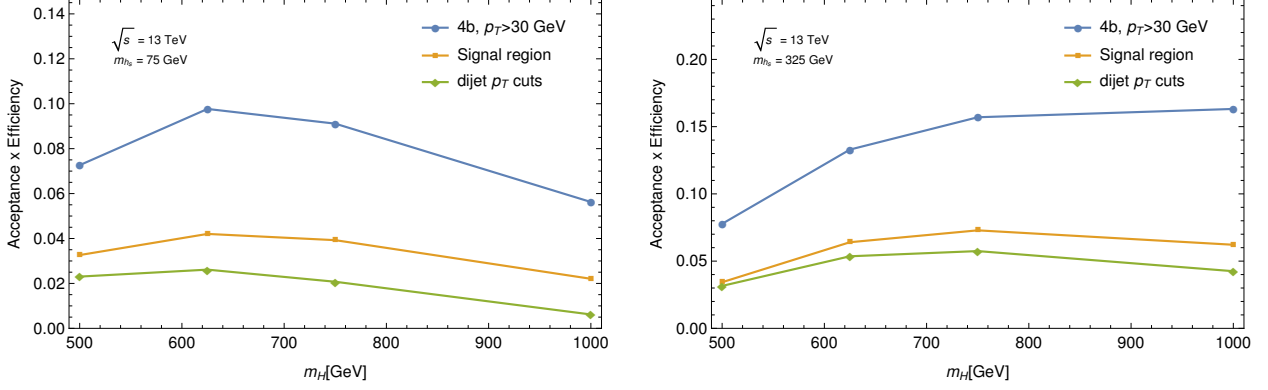


Figure 2: Efficiencies of the three cuts ($4b$ with $p_T > 30$ GeV), signal region (4.1) and dijet p_T (4.2) for $M_{H_S} = 75$ GeV and $M_{H_S} = 325$ GeV as function of M_H .

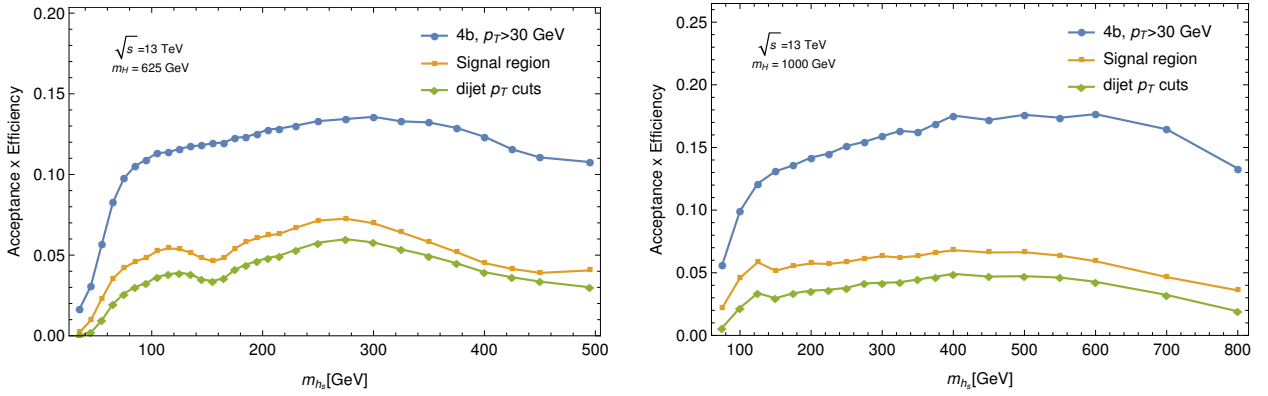


Figure 3: Efficiencies of the three cuts ($4b$ with $p_T > 30$ GeV), signal region (4.1) and dijet p_T (4.2) for $M_H = 625$ GeV and $M_H = 1000$ GeV as function of M_{H_S} .

4.2 Background Estimation

Dominant backgrounds for the $b\bar{b}b\bar{b}$ final state are QCD multijet processes including jet misidentifications, and $t\bar{t}$ [6, 14]. The QCD multijet background is difficult to obtain from Monte Carlo simulations alone, and estimated from sidebands in [6, 14]. Such data is not available for the different values of M_{H_S} studied here, with one exception: For $M_{H_S} \sim 125$ GeV, the $b\bar{b}b\bar{b}$ final state coincides with the one searched for in [6, 14].

We simulated $b\bar{b}b\bar{b}$, $b\bar{b}c\bar{c}$, $b\bar{b}j\bar{j}$ (with $j \neq c/\bar{c}$) and $t\bar{t}$ processes as we did for the signal samples in section 3. After applying the cuts of the previous subsection the relative contributions are $\sim 85 - 88\%$ from $b\bar{b}b\bar{b}$, $\sim 7 - 8\%$ from $b\bar{b}c\bar{c}$, $\sim 4 - 8\%$ from $t\bar{t}$ (depending on M_{H_S} and M_{4b}). The $b\bar{b}j\bar{j}$ contribution is only 0.8% and will subsequently be neglected. We checked that $b\bar{b}b\bar{b} + jets$ processes have little impact on the event shapes. Hence we did not simulate them separately, but took a NLO K-factor of 1.7 [38] into account.

In [6] the M_{4b} distribution of the multijet background has been obtained from a signal free sideband (with two b -tags only, and $M_{b\bar{b}}$ outside the search window) and appropriate rescaling using data with four b -tags, subtracting the $t\bar{t}$ contribution. The measured M_{4b} distribution is available in Fig. 5 in [6], where it is compared to the estimated background.

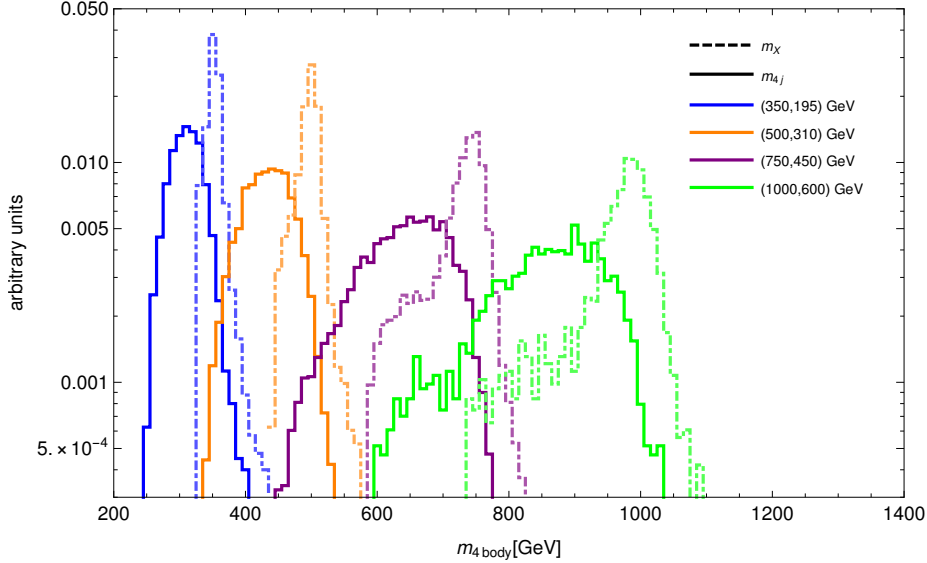


Figure 4: Distributions of the reconstructed masses M_{4b} (full lines) and M_X (dashed lines) for the signal samples $(M_H, M_{H_S}) = (350, 195), (500, 310), (750, 450), (1000, 600)$ GeV.

This allows us to proceed in a similar fashion: In order to compare to the data in [6], the previous cuts are slightly modified: The $b\bar{b}$ pairs are ordered in p_T according to $M_{b\bar{b}}^{lead}$ and $M_{b\bar{b}}^{subl}$ and, as in [6], the signal region is defined by

$$\chi = \sqrt{\left(\frac{M_{b\bar{b}}^{lead} - 120 \text{ GeV}}{0.1 M_{b\bar{b}}^{lead}}\right)^2 + \left(\frac{M_{b\bar{b}}^{subl} - 0.85 M_{H_S}}{0.1 M_{b\bar{b}}^{subl}}\right)^2} < 1.6 . \quad (4.4)$$

Still (and expectedly) our simulated background falls below the measured data given in [6]. On the left hand side of Fig. 5 we show the M_{4b} distribution measured by [6] using 10.1 fb^{-1} of integrated luminosity, and our MC result with statistical errors. The number of generated MC events corresponds to an equivalent integrated luminosity of $\sim 13 \text{ fb}^{-1}$. The statistical error per bin is thus obtained from the number of MC events per bin rescaled by $10/13$. The lower panels show the ratio MC/data bin by bin, with the uncertainties from the data and from our MC combined. At least for the interesting region $M_{4b} \gtrsim 350 \text{ GeV}$ an overall rescaling of our multijet background, like it was performed in [6], seems appropriate. The rescaling factor is obtained taking the average of the data/MC ratio of all bins weighted by the corresponding uncertainties. We obtain a rescaling factor of 1.55 ± 0.27 . (The $t\bar{t}$ background is left untouched, and remains at $\sim 3 - 6\%$.) The comparison of the M_{4b} distribution of our background after rescaling to the data from [6] is shown on the right hand side of Fig. 5.

Clearly it is somewhat optimistic to assume that the rescaling of the multijet background by 1.55 ± 0.27 remains valid for $M_{H_S} \neq 125 \text{ GeV}$. In the absence of data from sidebands this is, however, the best we can do. Subsequently ± 0.27 will be used as an estimation of the systematic uncertainty of our background for all M_{H_S} , a number to be considered as indicative.

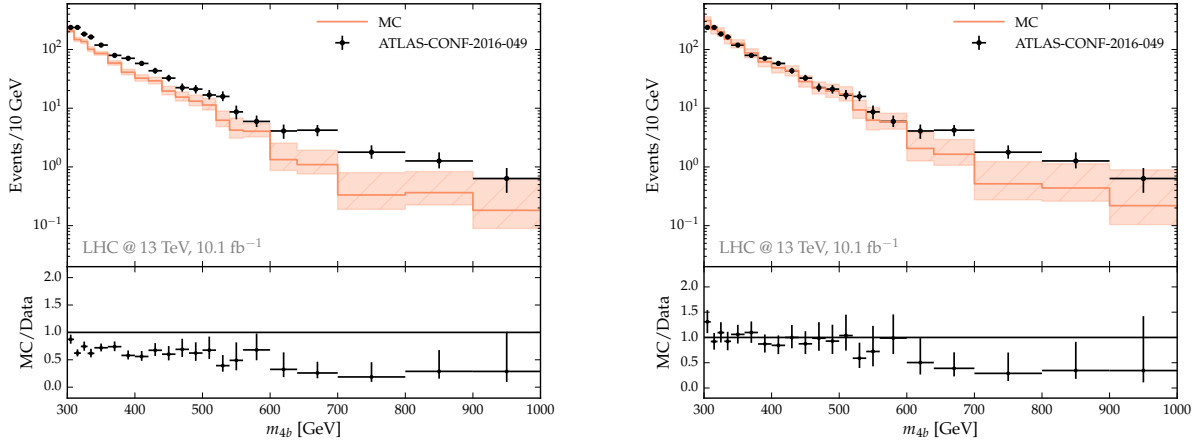


Figure 5: Left hand side: measured M_{4b} distribution from ATLAS-CONF-2016-049 [6], and our MC result for the background with statistical errors expected for 10.1 fb^{-1} of integrated luminosity. The lower part shows the ratio MC/data bin by bin. Right hand side: the M_{4b} distribution of our background after rescaling, compared to the data in ATLAS-CONF-2016-049 [6].

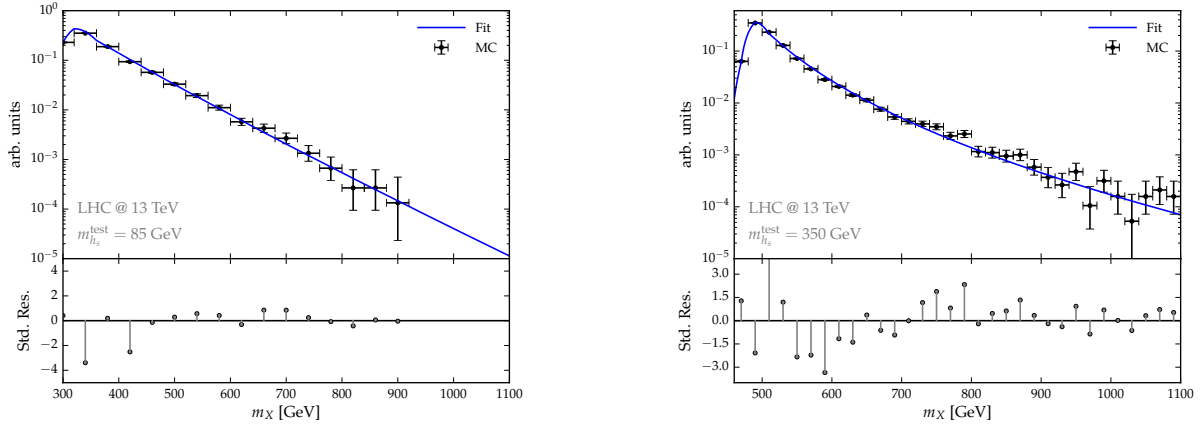


Figure 6: Fits by 4 parameter functions (A.1) to distributions of M_X of the background obtained by Monte Carlo simulations of $b\bar{b}b\bar{b}$, $b\bar{b}c\bar{c}$ and $t\bar{t}$ events after cuts, for $M_{H_S} = 85 \text{ GeV}$ (left) and $M_{H_S} = 350 \text{ GeV}$ (right). The indicated uncertainties originate from the Monte Carlo samples.

For forecasts at 300 or 3000 fb^{-1} integrated luminosity the statistical uncertainties of the background are much smaller. It is then convenient to fit the shape of the M_X background distributions (4.3) after cuts, which will be used in the following, by continuous functions. We found that the best fits are provided by a four parameter Gamma distribution defined in eq. (A.1) with M_{H_S} dependent fit parameters. (The $b\bar{b}b\bar{b}$, $b\bar{b}c\bar{c}$, and $t\bar{t}$ background contributions to the M_X distributions were fitted separately.) In Figs. 6 we show the sum of these fits for $M_{H_S} = 85 \text{ GeV}$ and $M_{H_S} = 350 \text{ GeV}$.

Of course the remaining statistical fluctuations of the background can still be evaluated

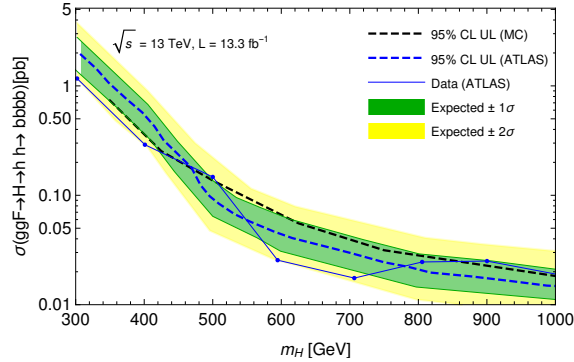


Figure 7: Expected 95% CL upper limits from ATLAS [6] in blue, their $\pm 2\sigma$ uncertainty bands, the expected 95% CL upper limits from our Monte Carlo in black and, for completeness, the 95% CL upper limits obtained from the data.

and combined with the systematic uncertainty (not shown in Figs. 6). It turns out, however, that for forecasts at 300 or 3000 fb^{-1} the statistical fluctuations are negligibly small relative to the systematic uncertainty from the rescaling by 1.55 ± 0.27 .

4.3 Future 95% CL Exclusion Limits and 5σ Discovery Cross Sections

Given the M_X distribution of the background for various hypothetical values of M_{H_S} and the M_X distributions of signals one can, following the statistical methods from [53] and described in the appendix B, obtain values for 95% CL exclusion limits and 5σ discovery limits for cross sections times branching fractions into the $b\bar{b}b\bar{b}$ final state as function of the integrated luminosity, M_H and M_{H_S} .

In the case of an integrated luminosity of 13.3 fb^{-1} at 13 TeV we can compare the expected 95% CL exclusion limits on cross sections times branching fractions to the ones given by ATLAS in Fig. 11 in [6], for $M_X = 300 \dots 1000$ GeV and $M_{H_S} \sim 125$ GeV. (This ATLAS search was actually dedicated to spin 2 resonances decaying to SM Higgs pairs, but the differences to spin-0 resonances are expected to be small.) In Fig. 7 we show the expected 95% CL upper limits from ATLAS, their $\pm 2\sigma$ uncertainty bands, the expected 95% CL upper limits from our Monte Carlo and, for completeness, the 95% CL upper limits obtained from the data. We see that our expected 95% CL upper limits coincide well with the ones expected by ATLAS.

Since the background was fitted to data at 13 TeV c.m. energy we will show our results also for 13 TeV, for 300 and 3000 fb^{-1} integrated luminosity. We choose four representative values for $M_H = 425, 500, 750$ and 1000 GeV, and show the 95% CL exclusion limits and 5σ discovery cross sections as function of M_{H_S} in each case. For 300 fb^{-1} integrated luminosity these are shown in Figs. 8, for 3000 fb^{-1} integrated luminosity in Figs. 9.

The expected limits become weaker for $M_{H_S} \lesssim 50$ GeV (for $M_X = 425 - 500$ GeV) and $M_{H_S} \lesssim 100$ GeV (for $M_H = 1000$ GeV). As stated in subsection 4.1 here the $b\bar{b}$ pair from H_S becomes too boosted and is no longer resolved by the standard jet clustering algorithm.

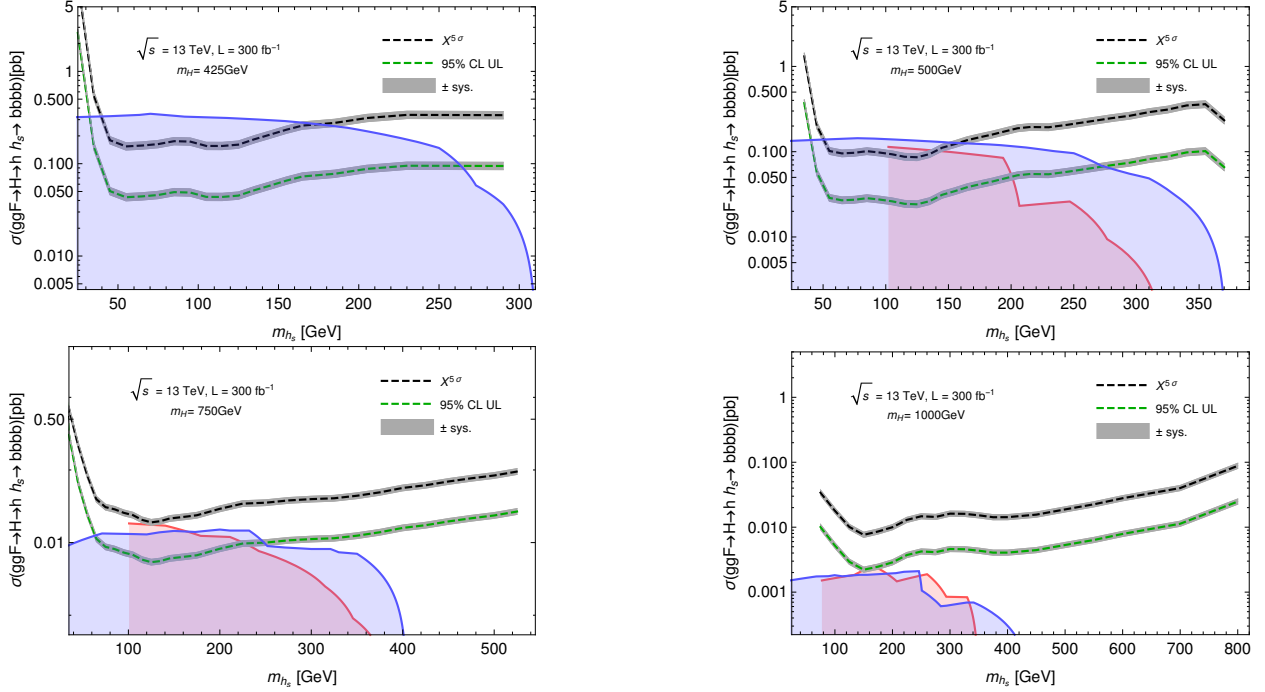


Figure 8: 95% CL exclusion limits and 5σ discovery cross sections in the $b\bar{b}b\bar{b}$ final state as function of M_{H_S} for 300 fb^{-1} integrated luminosity and $M_H = 425 \text{ GeV}$ (upper left), $M_H = 500 \text{ GeV}$ (upper right), $M_H = 750 \text{ GeV}$ (lower left), $M_H = 1000 \text{ GeV}$ (lower right). Shaded blue regions: viable values for $\sigma(ggF \rightarrow H \rightarrow H_{125} + H_S \rightarrow b\bar{b}b\bar{b})$ in the parameter space of the NMSSM. Shaded red regions: viable values for $\sigma(ggF \rightarrow A \rightarrow H_{125} + A_S \rightarrow b\bar{b}b\bar{b})$ in case they exceed potentially the ones for $\sigma(ggF \rightarrow H \rightarrow H_{125} + H_S \rightarrow b\bar{b}b\bar{b})$.

The shaded blue regions in Figs. 8 and 9 indicate viable values for the cross sections times branching fractions for $\sigma(ggF \rightarrow H \rightarrow H_{125} + H_S \rightarrow b\bar{b}b\bar{b})$ in the parameter space of the NMSSM, see section 2. Typically the viable values for $\sigma(ggF \rightarrow A \rightarrow H_{125} + A_S \rightarrow b\bar{b}b\bar{b})$ are smaller; if not we show them as shaded red regions. In the region of the NMSSM parameter space corresponding to $M_H \gtrsim 500 \text{ GeV}$, the partial width for $H_S \rightarrow H_{125} + H_{125}$ becomes relatively large ($\approx 10 \text{ MeV}$) if kinematically allowed. As a consequence the branching fractions of H_S into $b\bar{b}$ (and the other channels considered in this paper) decrease, leading to a decrease of the possible production cross sections times branching fractions for $M_H \gtrsim 500 \text{ GeV}$, $M_{H_S} \gtrsim 250 \text{ GeV}$.

The following conclusions can be drawn from Figs. 8 and 9: For $M_H \lesssim 500 \text{ GeV}$ wide ranges of M_{H_S} in the NMSSM parameter space can be discovered or, at least, excluded. For larger M_H testable regions in the NMSSM parameter space exist, but for $M_H \sim 1 \text{ TeV}$ only for 3000 fb^{-1} integrated luminosity. In fig. 10 we summarize these results showing the 95% C.L. expected upper limits in the M_H vs M_{H_S} plane.

We recall, however, that the sensitivities to cross sections in Figs. 8 and 9 are model independent and valid for arbitrary (e.g. non-supersymmetric) extensions of the Higgs sector.

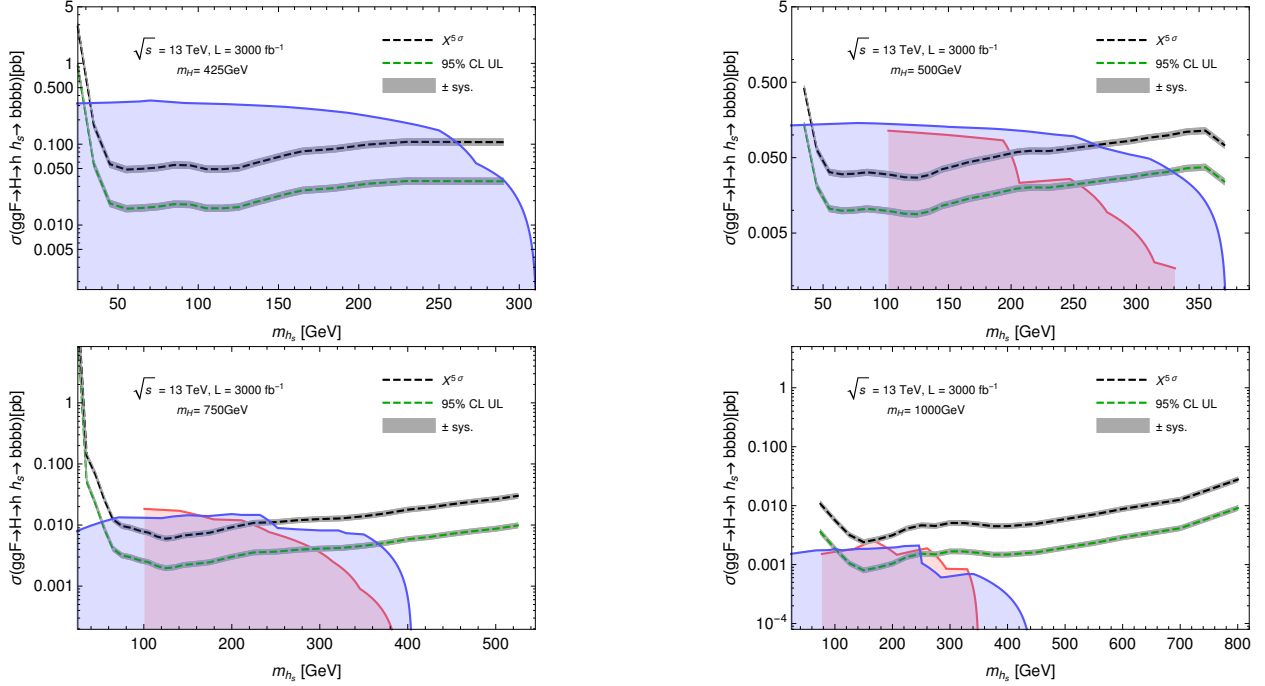


Figure 9: 95% CL exclusion limits and 5σ discovery cross sections in the $b\bar{b}b\bar{b}$ final state as function of M_{H_S} for 3000 fb^{-1} integrated luminosity and $M_H = 425\text{ GeV}$ (upper left), $M_H = 500\text{ GeV}$ (upper right), $M_H = 750\text{ GeV}$ (lower left), $M_H = 1000\text{ GeV}$ (lower right). The colored regions are explained in the caption of Fig. 8.

5 Search strategies for the $b\bar{b}\tau\tau$ final state

Searches for resonant H_{125} pair production in the $b\bar{b}\tau\tau$ final state have been performed by ATLAS at 8 TeV [4], and by CMS at 13 TeV in [16, 17, 19]. Following these searches we concentrate on the $\tau_h\tau_h$, $\tau_h\tau_e$ and $\tau_h\tau_\mu$ modes. As in the case of the $b\bar{b}b\bar{b}$ final state we optimise the cuts as function of a tentative value for M_{H_S} .

A priori the $\tau\tau$ pair can originate from H_S or H_{125} ; both cases will be studied below. For the analysis we will make no assumptions on the relative branching ratios $BR(H_S \rightarrow b\bar{b})$ and $BR(H_S \rightarrow \tau\tau)$. The aim is to obtain separate 95% CL exclusion limits and 5σ discovery cross sections for the processes $ggF \rightarrow H \rightarrow H_S(\rightarrow b\bar{b}) + H_{125}(\rightarrow \tau\tau)$, and $ggF \rightarrow H \rightarrow H_S(\rightarrow \tau\tau) + H_{125}(\rightarrow b\bar{b})$.

5.1 Analyses of Signal Samples

For the simulation of signal samples the same series of codes as for the $b\bar{b}b\bar{b}$ final state was used, see section 3. Events are required to have exactly two b -tagged jets with $p_T(b) > 30\text{ GeV}$ and $|\eta| < 2.5$. For the b -tagging efficiency a working point with $\varepsilon_b = 70\%$ is chosen. If the event has exactly two hadronic taus τ_h , both are required to have $p_T(\tau_h) > 45\text{ GeV}$. Events with one hadronic tau are required to have exactly one additional isolated lepton $\ell = e, \mu$ of

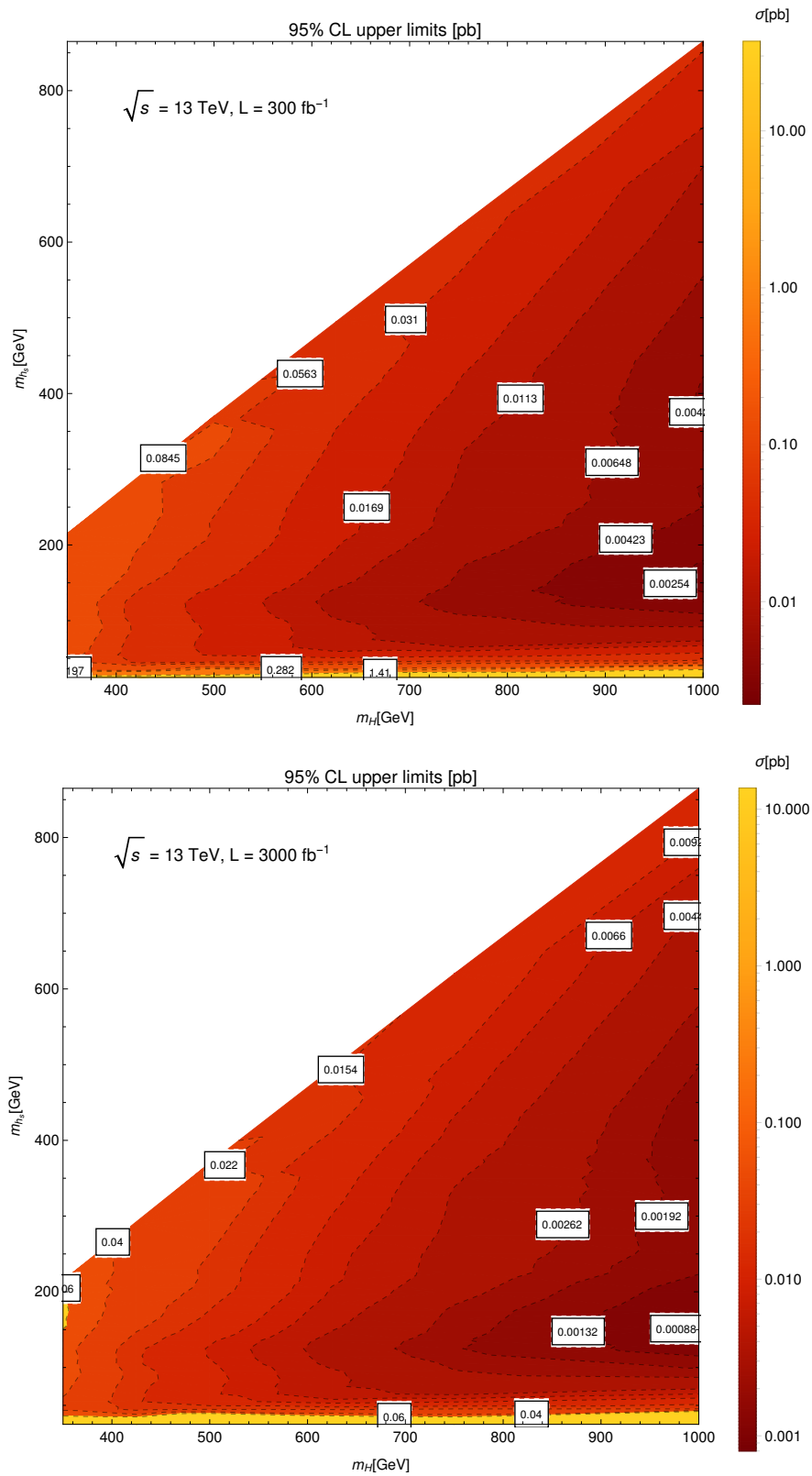


Figure 10: 95% CL expected upper limits for the process $H \rightarrow H_{125}H_S \rightarrow \bar{b}b\bar{b}b$ for $L=300 \text{ fb}^{-1}$ (end of Run III) (up) and $L=3000 \text{ fb}^{-1}$ (HL-LHC).

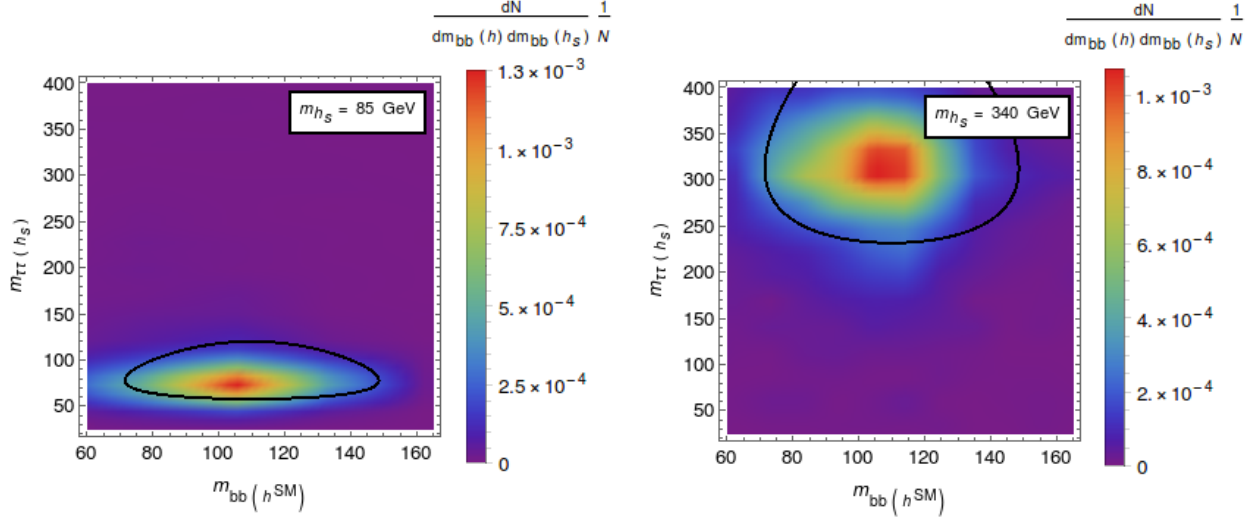


Figure 11: Dijet mass distributions $M_{b\bar{b}}(H_{125})$ and $M_{\tau\tau}(H_S)$ for two different benchmark points $M_{H_S} = 85$ GeV and $M_{H_S} = 340$ GeV. The black contours indicate the signal regions defined by $\chi < 1$.

opposite charge and with $p_T(\ell) > 20$ GeV. For the transverse mass m_T^ℓ of leptons we require

$$m_T^\ell \equiv \sqrt{2p_T(\ell)E_T^{miss}(1 - \cos(\phi(E_T^{miss}) - \phi(\ell)))} < 40 \text{ GeV} . \quad (5.1)$$

All objects are required to have $|\eta| < 2.47$. In the case of $\tau_h\tau_\ell$ final states the invariant mass $M_{\tau\tau}$ was reconstructed using the collinear mass, i.e. assuming that the neutrino from the τ_ℓ decay is emitted collinear to the lepton and responsible for all E_T^{miss} .

Considering first the case where the $\tau\tau$ pair originates from H_S with an assumed mass M_{H_S} (and hence that $M_{b\bar{b}}$ should be close to 125 GeV), a M_{H_S} dependent signal region is defined by

$$\chi = \sqrt{\left(\frac{M_{b\bar{b}} - 110 \text{ GeV}}{0.35 \cdot M_{b\bar{b}}}\right)^2 + \left(\frac{M_{\tau\tau} - 0.92 \cdot M_{H_S}}{\text{Max}(0.35 \cdot M_{\tau\tau}, 30 \text{ GeV})}\right)^2} < 1 . \quad (5.2)$$

If different pairings within a given event satisfy (5.2), the combination that minimizes χ is chosen. In Figs. 11 we show, for $M_H = 500$ GeV, the distributions of the dijet mass $M_{b\bar{b}}(H_{125})$ and $M_{\tau\tau}(H_S)$ for the pairing minimizing χ , for two different benchmark points $M_{H_S} = 85$ GeV and $M_{H_S} = 340$ GeV in the case where M_{H_S} for the analysis was chosen correctly. The black contours indicate the signal regions defined by $\chi < 1$.

Cuts on the transverse momenta of Higgs candidates are chosen as

$$\begin{aligned} p_T(b\bar{b}) &> 52 \text{ GeV} + 0.14 M_X - 0.2 M_{H_S} - \frac{M_{H_S}}{M_X} \cdot 202 \text{ GeV} \\ p_T(\tau\tau) &> 24 \text{ GeV} + 0.19 M_X - 0.02 M_{H_S} - \frac{M_{H_S}}{M_X} \cdot 128 \text{ GeV} \end{aligned} \quad (5.3)$$

with

$$M_X = M_{b\bar{b}\tau\tau} + 125 \text{ GeV} - M_{b\bar{b}} . \quad (5.4)$$

The numerical coefficients in eqs. (5.2)–(5.4) were obtained by optimizing the relative signal to background efficiency.

In the case where the $b\bar{b}$ pair originates from H_S with an assumed mass M_{H_S} (and hence that $M_{\tau\tau}$ should be close to 125 GeV), the signal region (5.2) is replaced by

$$\chi = \sqrt{\left(\frac{M_{\tau\tau} - 120 \text{ GeV}}{0.35 \cdot 120 \text{ GeV}}\right)^2 + \left(\frac{M_{b\bar{b}} - 0.85 \cdot M_{H_S}}{\text{Max}(0.35 \cdot M_{H_S}, 35 \text{ GeV})}\right)^2} < 1 \quad (5.5)$$

and the cuts on the transverse momenta of Higgs candidates are

$$\begin{aligned} p_T(\tau\tau) &> 118 \text{ GeV} + 0.02 M_X - 0.55 M_{H_S} - \frac{M_{H_S}}{M_X} \cdot 380 \text{ GeV} \\ p_T(b\bar{b}) &> 16 \text{ GeV} + 0.19 M_X - 0.02 M_{H_S} - \frac{M_{H_S}}{M_X} \cdot 137 \text{ GeV} \end{aligned} \quad (5.6)$$

with

$$M_X = M_{b\bar{b}\tau\tau} + M_{H_S} - M_{b\bar{b}}. \quad (5.7)$$

Hence, for each tentative value of M_{H_S} two different analyses using different cuts are to be performed, resulting in two (slightly) different distributions of M_X .

5.2 Background Estimation

Backgrounds originate from $t\bar{t}$ (and single top) and QCD+electroweak $b\bar{b}\tau\tau$ production. Contributions from one or more jets misidentified as τ_h are seen to become small after the cuts on $p_T(\tau\tau)$. We have generated $1.5 \cdot 10^7$ $t\bar{t}$ events using `MadGraph5_aMC@NLO` [38]; the LO cross section was rescaled by a (NNLO+NNLL) K-factor 1.7 obtained from `top++2.0` [47–52]. `MadGraph5_aMC@NLO` was also used to generate QCD+electroweak $b\bar{b}\tau\tau$ events; the LO cross section was rescaled by a NLO K-factor 2.9.

After applying the cuts of the previous subsection, the relative contributions of the SM backgrounds depend on M_{H_S} and on whether the $\tau\tau$ pair originates from H_S or H_{125} , although $t\bar{t}$ is always dominant: For $H_S \rightarrow \tau\tau$ the $t\bar{t}$ contribution increases from $\sim 60\%$ for $M_{H_S} \sim 50$ GeV to $\sim 100\%$ for $M_{H_S} \gtrsim 350$ GeV, the remaining background stems from QCD+electroweak $b\bar{b}\tau\tau$ production. For $H_{125} \rightarrow \tau\tau$ the $t\bar{t}$ contribution is always $\sim 90\%$.

In order to validate the background contribution to the M_X distribution after cuts we use again a search for H_{125} pair production at 13 TeV, now in the $b\bar{b}\tau\tau$ channel. Measurements of distributions of the (slightly corrected) total invariant mass by CMS, separately in the $b\bar{b}e\tau_h$, $b\bar{b}\mu\tau_h$ and $b\bar{b}\tau_h\tau_h$ channels, can be found in Fig. 1 in [17].

We have reproduced the cuts in [17] using our background samples. In Figs. 12 we show the measured total invariant mass distribution from Fig. 1 in [17] in black, and our MC results including the statistical uncertainties corresponding to 12.9 fb^{-1} of integrated luminosity, in the three channels, in orange. Due to the smaller number of events the statistical uncertainties are now larger than in the $4b$ case.

Still we can ask which rescaling of our simulated background, independent of the total invariant mass and common to all three channels (to improve the statistics), provides a best

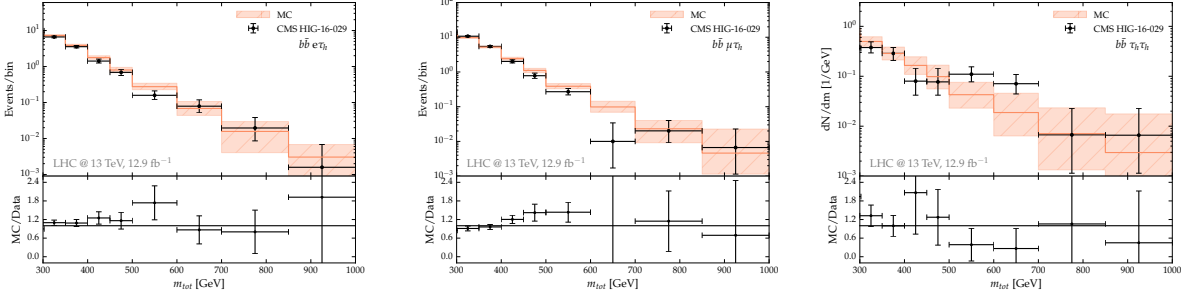


Figure 12: Measured total invariant mass distribution from [17] in black, and our MC results in orange including the statistical uncertainties corresponding to 12.9 fb^{-1} of integrated luminosity in the three channels $b\bar{b}e\tau_h$, $b\bar{b}\mu\tau_h$ and $b\bar{b}\tau_h\tau_h$.

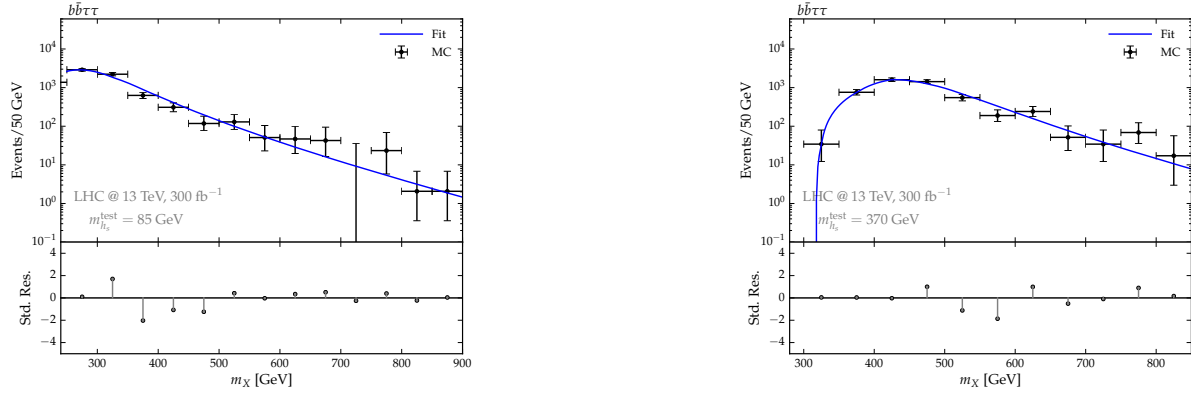


Figure 13: Fits to distributions of M_X of the background obtained by Monte Carlo simulations of $t\bar{t}$ and $b\bar{b}\tau\tau$ events after cuts eq. 5.1–5.3 corresponding to $M_{H_S} = 85 \text{ GeV}$ (left) and $M_{H_S} = 370 \text{ GeV}$ (right). The indicated uncertainties originate from the Monte Carlo samples.

fit to the data. We find a factor 1.01 ± 0.24 , and will subsequently use ± 0.24 as an estimate of the systematic uncertainty of the background normalisation.

For forecasts at 300 or 3000 fb^{-1} integrated luminosity the shape of the M_X background distributions (5.4) will again be parametrized by continuous functions with M_{H_S} dependent parameters: For the $t\bar{t}$ background the Frechet distribution, and for the $b\bar{b}\tau\tau$ background (all channels combined) the GaussExp function already used in [14]. Both functions are defined in the appendix A. In Figs. 13 we show these fits for $M_{H_S} = 85 \text{ GeV}$ and $M_{H_S} = 350 \text{ GeV}$ where the $\tau\tau$ pair originates from H_S .

5.3 Future 95% CL Exclusion Limits and 5σ Discovery Cross Sections

Given the M_X distribution of the background for various hypothetical values of M_{H_S} and the M_X distributions of signals we can, as before, obtain values for 95% CL exclusion and 5σ discovery for cross sections times branching fractions into the $H_{125} \rightarrow b\bar{b}$, $H_S \rightarrow \tau\tau$ and

$H_{125} \rightarrow \tau\tau$, $H_S \rightarrow b\bar{b}$ final states as function of the integrated luminosity, M_H and M_{H_S} . We choose four representative values for $M_H = 425, 500, 750$ and 1000 GeV, and show the 95% CL exclusion limits and 5σ discovery cross sections as function of M_{H_S} in each case. For $H_{125} \rightarrow b\bar{b}$, $H_S \rightarrow \tau\tau$ at 300 fb^{-1} integrated luminosity these are shown in Figs. 14, for 3000 fb^{-1} integrated luminosity in Figs. 15. For $H_{125} \rightarrow \tau\tau$, $H_S \rightarrow b\bar{b}$ at 300 fb^{-1} integrated luminosity these are shown in Figs. 16, for 3000 fb^{-1} integrated luminosity in Figs. 17. The uncertainties include statistical uncertainties and, added linearly, ± 0.24 considered as an estimate of the systematic uncertainty originating from the normalisation of the background.

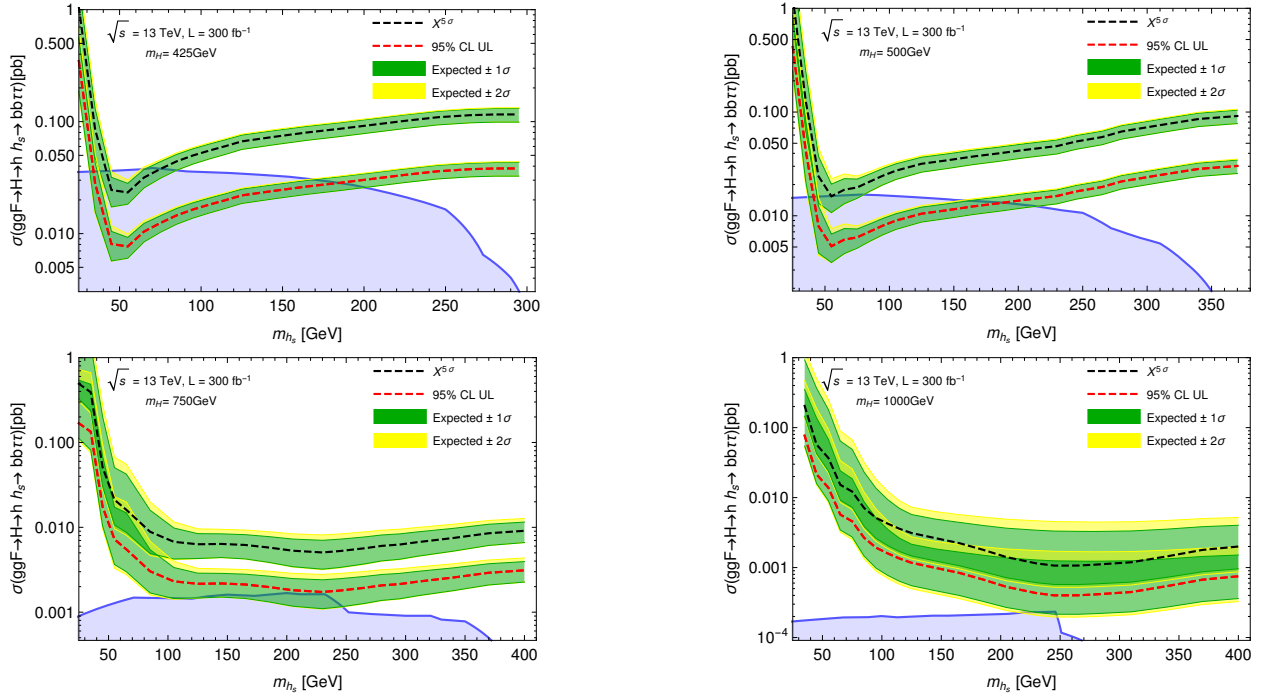


Figure 14: 95% CL exclusion limits and 5σ discovery cross sections for $H_{125} \rightarrow b\bar{b}$ and $H_S \rightarrow \tau\tau$ as function of M_{H_S} for 300 fb^{-1} integrated luminosity and $M_H = 425$ GeV (upper left), $M_H = 500$ GeV (upper right), $M_H = 750$ GeV (lower left), $M_H = 1000$ GeV (lower right).

The following observations can be made: First, the expected sensitivities on cross sections times branching ratios differ hardly among the cases $H_{125} \rightarrow b\bar{b}$ and $H_S \rightarrow \tau\tau$ versus $H_{125} \rightarrow \tau\tau$ and $H_S \rightarrow b\bar{b}$; if at all, the analyses aiming at $H_{125} \rightarrow b\bar{b}$ and $H_S \rightarrow \tau\tau$ are typically somewhat more sensitive.

Second, in Two-Higgs-Doublet models of type II as well as in the NMSSM the branching fractions into $b\bar{b}$ and $\tau\tau$ of both H_{125} and H_S are always related by a factor $\sim 9 : 1$. Accordingly the possible cross sections times branching fractions in the NMSSM parameter space for both $\sigma(ggF \rightarrow H \rightarrow H_{125} + H_S \rightarrow b\bar{b}\tau\tau)$ and $\sigma(ggF \rightarrow H \rightarrow H_{125} + H_S \rightarrow \tau\tau b\bar{b})$, indicated in blue in Figs. 14 – 17, are $\sim 1/9$ of the ones in Figs. 8 – 9 for the $b\bar{b}b\bar{b}$ final state. (The same reasoning applies to $\sigma(ggF \rightarrow A \rightarrow H_{125} + A_S \rightarrow b\bar{b}\tau\tau)$ and $\sigma(ggF \rightarrow A \rightarrow H_{125} + A_S \rightarrow \tau\tau b\bar{b})$; the viable NMSSM points correspond to the ones in Figs. 8 and 9.)

Then one can ask, for a given point in parameter space, which of the analyses considered up to now is the most sensitive. According to our results this is the search in the $b\bar{b}b\bar{b}$ final

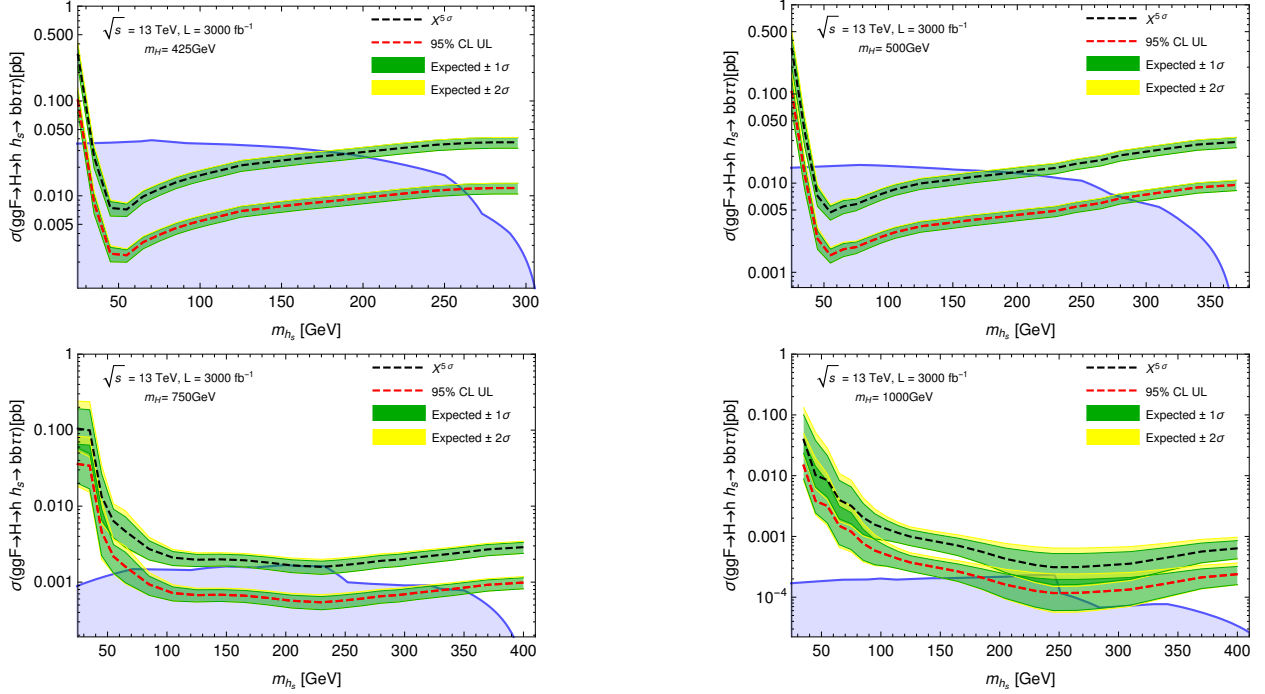


Figure 15: 95% CL exclusion limits and 5σ discovery cross sections for $H_{125} \rightarrow b\bar{b}$ and $H_S \rightarrow \tau\tau$ as function of M_{H_S} for 3000 fb^{-1} integrated luminosity and $M_H = 425 \text{ GeV}$ (upper left), $M_H = 500 \text{ GeV}$ (upper right), $M_H = 750 \text{ GeV}$ (lower left), $M_H = 1000 \text{ GeV}$ (lower right).

state which allows to test somewhat larger regions in parameter space.

6 Search strategies for the $b\bar{b}\gamma\gamma$ final state

Searches for resonant H_{125} pair production in the $b\bar{b}\gamma\gamma$ final state have been performed by ATLAS at 8 TeV [2,4] and at 13 TeV [5], by CMS at 8 TeV in [7] and at 13 TeV in [18,21]. A priori the diphotons can originate from H_S or H_{125} ; both cases will be studied below. As in case of the previous final states we optimise the cuts as function of a tentative value for M_{H_S} .

6.1 Analyses of Signal Samples

For the simulation of signal samples we used again MadGraph5_aMC@NLO [38]. Events are required to have exactly two b -tagged jets with $p_T(b) > 40 \text{ GeV}$ and $|\eta| < 2.5$. Following ATLAS [5] a working point with $\epsilon_b = 0.85$ was chosen for the b -tagging efficiency in order to increase the statistics.

At least two photons are required in each event which have to satisfy the isolation criteria

$$\frac{\sum_i p_{T,i}}{p_{T,\gamma}} < 0.1 \quad (6.1)$$

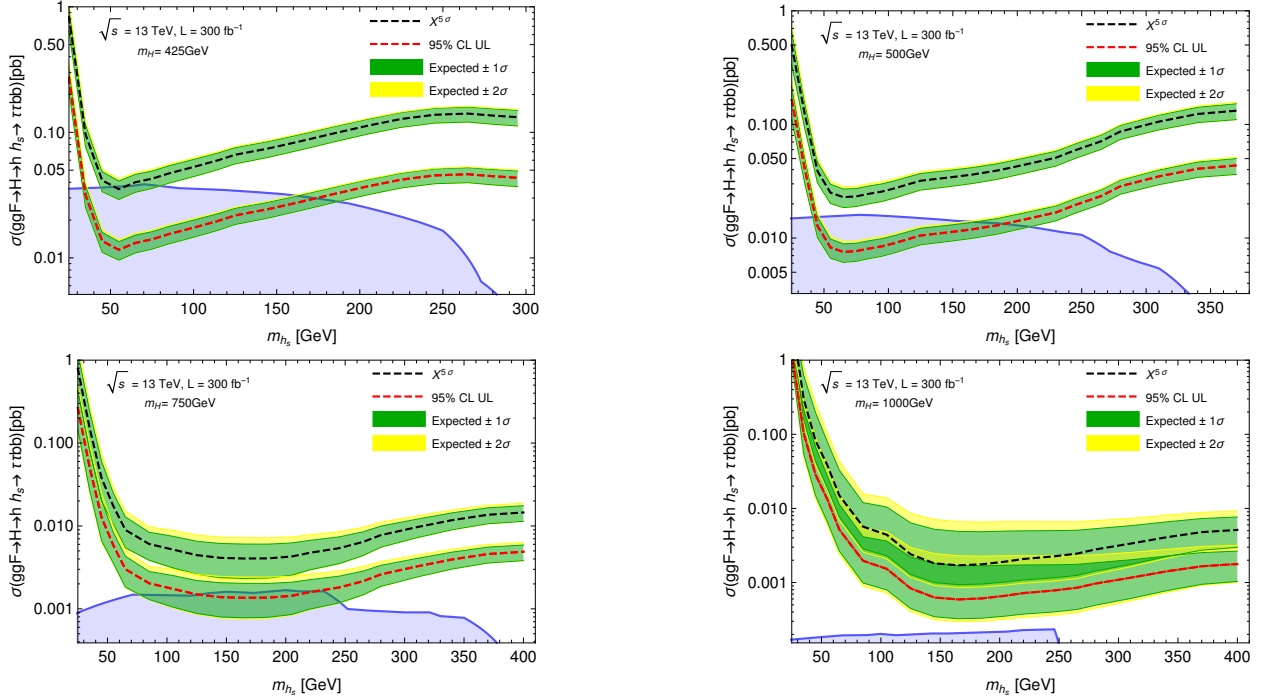


Figure 16: 95% CL exclusion limits and 5σ discovery cross sections for $H_{125} \rightarrow \tau\tau$ and $H_S \rightarrow b\bar{b}$ as function of M_{H_S} for 300 fb^{-1} integrated luminosity and $M_H = 425 \text{ GeV}$ (upper left), $M_H = 500 \text{ GeV}$ (upper right), $M_H = 750 \text{ GeV}$ (lower left), $M_H = 1000 \text{ GeV}$ (lower right).

where the sum over i includes all tracks within a cone $\Delta R = 0.4$ around the photon. The two leading photons are required to satisfy

$$E_T^{\text{lead}}/M_{\gamma\gamma} > 0.35, \quad E_T^{\text{subl}}/M_{\gamma\gamma} > 0.25, \quad |\eta| < 2.37. \quad (6.2)$$

Additional cuts depend on whether the diphoton pair is assumed to originate from H_{125} or H_S , and the assumed value of M_{H_S} . First we consider the case $H_S \rightarrow \gamma\gamma$. Then the $b\bar{b}$ pair is assumed to originate from H_{125} , and we require

$$100 \text{ GeV} < M_{b\bar{b}} < 150 \text{ GeV}. \quad (6.3)$$

As in the previous cases it is useful to define a corrected invariant mass M_X for the $b\bar{b}\gamma\gamma$ system:

$$M_X = M_{b\bar{b}\gamma\gamma} + 125 \text{ GeV} - M_{b\bar{b}}. \quad (6.4)$$

Given an assumed value for M_{H_S} it turned out to optimize the signal to background efficiency applying a M_X and M_{H_S} dependent cut on the diphoton invariant mass $M_{\gamma\gamma}$, since the measured distribution $|M_{\gamma\gamma} - M_{H_S}|$ broadens somewhat with M_X :

$$|M_{\gamma\gamma} - M_{H_S}| < 4.3 \text{ GeV} + 0.016M_X. \quad (6.5)$$

Also the cuts on the H_{125} and H_S candidates depend on M_X :

$$p_T(b\bar{b}) > 17 \text{ GeV} + 0.18M_X, \quad (6.6)$$

$$E_T(\gamma\gamma) = 68.3 \text{ GeV} + 0.25M_X. \quad (6.7)$$

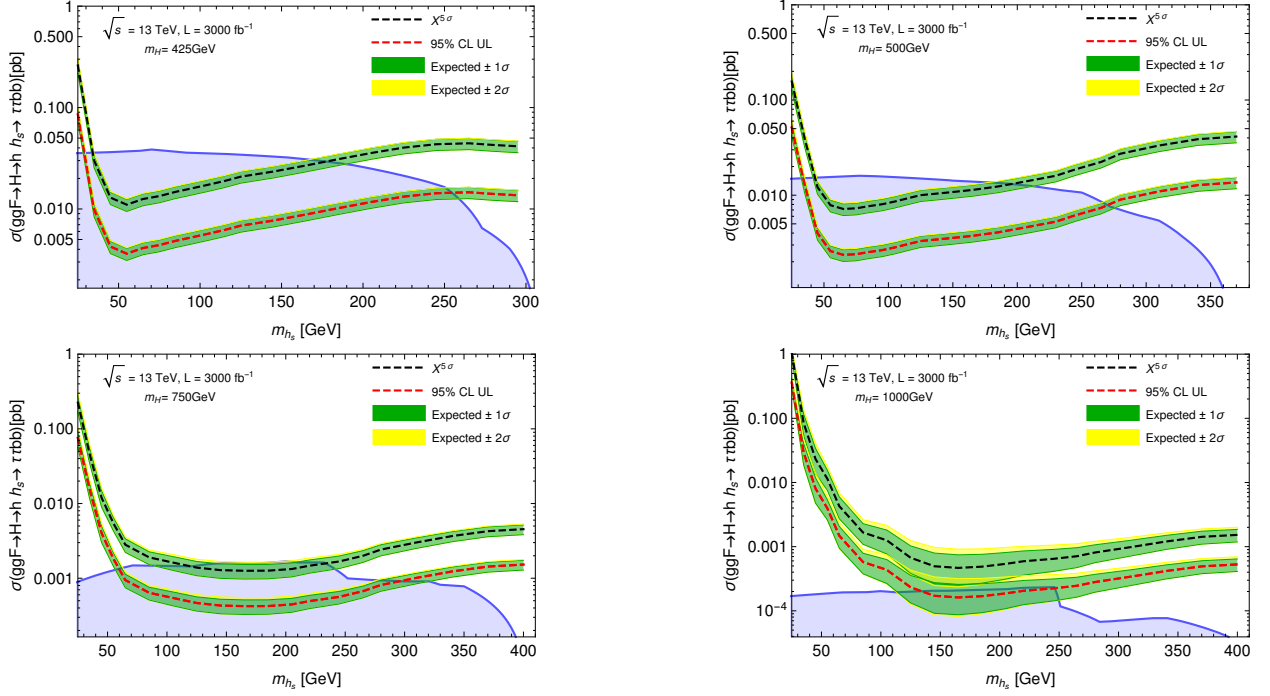


Figure 17: 95% CL exclusion limits and 5σ discovery cross sections for $H_{125} \rightarrow \tau\tau$ and $H_S \rightarrow b\bar{b}$ as function of M_{H_S} for 3000 fb^{-1} integrated luminosity and $M_H = 425 \text{ GeV}$ (upper left), $M_H = 500 \text{ GeV}$ (upper right), $M_H = 750 \text{ GeV}$ (lower left), $M_H = 1000 \text{ GeV}$ (lower right).

($E_T(\gamma\gamma)$ instead of $p_T(\gamma\gamma)$ allows for M_{H_S} independent cuts.)

Assuming $H_{125} \rightarrow \gamma\gamma$ and $H_S \rightarrow b\bar{b}$ the previous cuts are modified as follows: First, for M_X we take

$$M_X = M_{b\bar{b}\gamma\gamma} + M_{H_S} - M_{b\bar{b}}, \quad (6.8)$$

and for the diphoton invariant mass we require

$$|M_{\gamma\gamma} - 125 \text{ GeV}| < 2 \text{ GeV} + 0.02M_X. \quad (6.9)$$

The mass window for $M_{b\bar{b}}$ is now

$$0.9M_{H_S} - 30 \text{ GeV} < M_{b\bar{b}} < 0.9M_{H_S} + 20 \text{ GeV}. \quad (6.10)$$

The cuts on the H_{125} and H_S candidates are:

$$p_T(b\bar{b}) > -5.7 \text{ GeV} + 0.29M_X, \quad (6.11)$$

$$E_T(\gamma\gamma) = 7.45 \text{ GeV} + 0.33M_X. \quad (6.12)$$

All the numerical values above have been obtained by optimising signal-to-background ratios using the MC events.

6.2 Background Estimation

SM backgrounds originate from $b\bar{b}\gamma\gamma$, $c\bar{c}\gamma\gamma$, $jj\gamma\gamma$ ($j \neq c/\bar{c}$), $b\bar{b}j\gamma$ and $t\bar{t}H$. We simulated these backgrounds again using MadGraph5_aMC@NLO. Due to the relatively large b -tagging

efficiency $\epsilon = 0.85$ mistagging rates are relatively large. $b\bar{b}j\gamma$ contribute if another fake photon appears.

After applying the cuts of the previous subsection the relative contributions of the SM backgrounds depend strongly on M_{H_S} and M_H , and on whether the $\gamma\gamma$ pair originates from H_S or H_{125} . For a light $H_S \sim 85$ GeV the background from $b\bar{b}j\gamma$ is always important, $\sim 60\%$ for $H_S \rightarrow \gamma\gamma$ and $\sim 30\%$ for $H_S \rightarrow b\bar{b}$. However, all other $\gamma\gamma + X$ SM backgrounds can also contribute several 10% individually. The contribution from $t\bar{t}H$ is always $\lesssim 3\%$.

For $b\bar{b}\gamma\gamma$, $c\bar{c}\gamma\gamma$ and $j\bar{j}\gamma\gamma$ an extra jet was allowed in the final state, $b\bar{b}j\gamma$ was multiplied by a NLO K factor 1.58 from [38], and $t\bar{t}H$ (with SM couplings) was simulated at NLO.

Still we cannot expect that the total SM background cross section is completely captured by the MC simulation; in searches by ATLAS and CMS in [5, 18, 21] sidebands are used for this purpose. Thus we proceed as before and correct the total background cross section using data driven methods in the particular case $M_{H_S} \sim 125$ GeV equivalent to (resonant) SM Higgs pair production. To this end we modify slightly the cuts on $p_T(b)$ (> 55 GeV and > 35 GeV for the leading and next-to-leading b -jets), $M_{b\bar{b}}$ and $M_{\gamma\gamma}$ such that they coincide with the ones in the ATLAS search [5]. (In the case of $M_{\gamma\gamma}$ we could check that the efficiency coincides.) Extrapolating from sidebands with less b -jets, ATLAS [5] obtained 1.63 ± 0.3 expected background events in the signal region, whereas we found 1.06 ± 0.14 events from summing all MC events. Since all our backgrounds were simulated to similar order (NLO) in the QCD coupling and separate higher order K factors are not available, we multiply their sum by 1.54 ± 0.35 where the latter uncertainty will again be treated as an estimate of the systematic uncertainty contributing to our final results.

The dependence of the background on the total invariant mass $M_{b\bar{b}\gamma\gamma}$ was parametrized in [5] by a two parameter Landau distribution given in appendix A. We found that the Landau distribution fits the M_X distribution from eq. (6.8) as well (with M_{H_S} dependent parameters), and used it for the expected M_X distributions of the various background contributions for our forecasts at 300 fb^{-1} and 3000 fb^{-1} .

6.3 Future 95% CL Exclusion Limits and 5σ Discovery Cross Sections

Given the M_X distribution of the background for various hypothetical values of M_{H_S} and the M_X distributions of signals we can, as before, obtain values for 95% CL exclusion and 5σ discovery for cross sections times branching fractions into the $H_{125} \rightarrow b\bar{b}$, $H_S \rightarrow \gamma\gamma$ and $H_{125} \rightarrow \gamma\gamma$, $H_S \rightarrow b\bar{b}$ final states as function of the integrated luminosity, M_H and M_{H_S} .

After completing our analysis the CMS search [21] for resonant Higgs pair production in the channel $H_{125}+H_{125} \rightarrow b\bar{b}\gamma\gamma$ based on 35.9 fb^{-1} appeared. The expected 95% CL exclusion limits given in [21] can be compared to ours for $M_{H_S} = 125$ GeV for the same integrated luminosity; this comparison as function of M_H is shown in Fig. 18. The expected limits coincide within 1σ for $M_H \gtrsim 500$ GeV, and within 2σ everywhere. Our expected limits are systematically more conservative; we note that the CMS analysis employs a trained boosted decision tree in order to separate the signal from the backgrounds which is not available here.

Our expected 95% CL exclusion limits and 5σ discovery cross sections for $H_{125} \rightarrow b\bar{b}$,

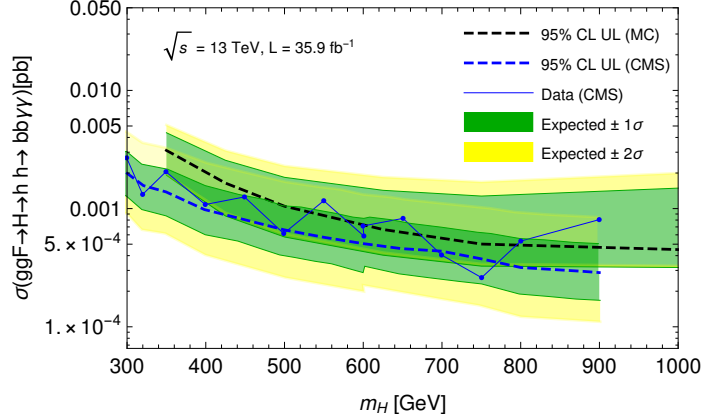


Figure 18: Expected 95% CL exclusion limits for $ggF \rightarrow H_{125}H_{125} \rightarrow b\bar{b}\gamma\gamma$ for 35.9 fb^{-1} from CMS [21] and from our MC simulation as function of M_H . For completeness the observed limits are shown.

$H_S \rightarrow \gamma\gamma$ as function of M_{H_S} at 300 fb^{-1} integrated luminosity are shown in Figs. 19 for four representative values for $M_H = 425, 500, 625$ and 750 GeV , and for 3000 fb^{-1} integrated luminosity in Figs. 20. For $H_{125} \rightarrow \gamma\gamma$, $H_S \rightarrow b\bar{b}$ at 300 fb^{-1} integrated luminosity these are shown in Figs. 21, for 3000 fb^{-1} integrated luminosity in Figs. 22. As in the $b\bar{b}b\bar{b}$ case, we also present the results for the expected 95% C.L. upper limits in the $M_{H_{125}}$ vs M_{H_S} plane in fig. 23.

The uncertainties include statistical uncertainties and, added linearly, a factor ± 0.35 considered as systematic uncertainty originating from the normalisation of the background.

As before viable NMSSM regions for scalar production are shown in shaded blue, for pseudoscalar production in shaded red in case they potentially exceed the ones for scalar production. Again a sizeable region in the NMSSM parameter space can be tested in this final state provided M_H is not too large. It is, however, *not* the same region potentially visible in the $b\bar{b}b\bar{b}$ final state: The branching fraction of H_S into $\gamma\gamma$ can vary in the $0.2\% \pm 0.1\%$ range, and is anticorrelated with its branching fraction into $b\bar{b}$. Moreover, as it is visible from the shaded red regions in Figs. 19 and 20, the signal rates $\sigma(ggF \rightarrow A \rightarrow H_{125} + A_S \rightarrow b\bar{b}\gamma\gamma)$ can be relatively large. These correspond to very singlet-like pseudoscalars A_S with very suppressed couplings to quarks and leptons, but sizeable coupling $\sim \lambda$ to higgsinos. Then the charged higgsino-loop induced coupling to diphotons can dominate, leading to a large $BR(A_S \rightarrow \gamma\gamma)$. The coupling $A - A_S - H_{125}$ is *not* suppressed in this case, leading to potentially large signal rates.

On the experimental side, the comparison of the upper limits on $H_{125} \rightarrow b\bar{b}$ and $H_S/A_S \rightarrow \gamma\gamma$ versus $H_{125} \rightarrow \gamma\gamma$ and $H_S/A_S \rightarrow b\bar{b}$ has a simple answer depending on M_{H_S/A_S} : For $M_{H_S/A_S} < 125 \text{ GeV}$ the search for $H_S/A_S \rightarrow \gamma\gamma$ is sensitive to smaller signal rates, whereas for $M_{H_S/A_S} > 125 \text{ GeV}$ the search for $H_{125} \rightarrow \gamma\gamma$, $H_S/A_S \rightarrow b\bar{b}$ is typically sensitive to smaller signal rates. However, different regions in the parameter space of underlying models are tested by these searches.

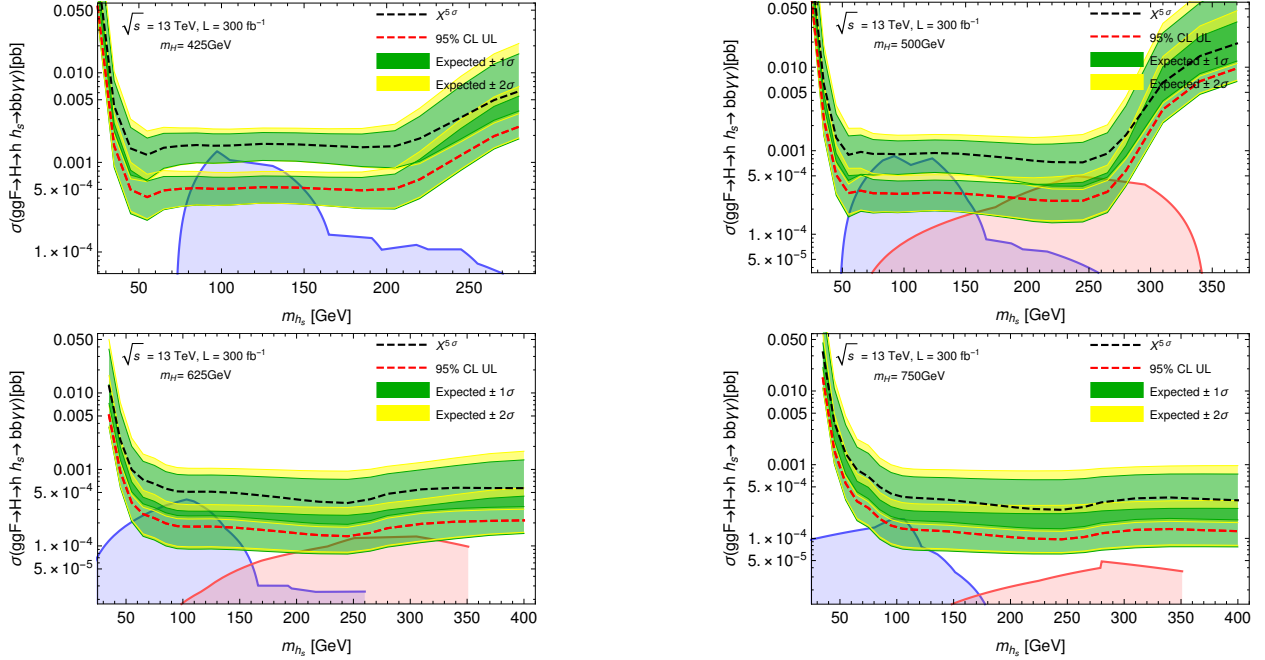


Figure 19: 95% CL exclusion limits and 5σ discovery cross sections for $H_{125} \rightarrow b\bar{b}$ and $H_S \rightarrow \gamma\gamma$ as function of M_{H_S} for 300 fb^{-1} integrated luminosity and $M_H = 425$ GeV (upper left), $M_H = 500$ GeV (upper right), $M_H = 625$ GeV (lower left), $M_H = 750$ GeV (lower right). The colored regions are explained in the caption of Fig. 8.

7 Conclusions and Outlook

Searches for resonant SM Higgs pair production are performed with considerable effort by ATLAS and CMS. As explained in the introduction searches for $ggF \rightarrow \Phi \rightarrow H_1 + H_2$ can be more promising where either H_1 or H_2 can be SM-like, and the other state being possibly CP-odd (which does not affect the search methods).

This scenario is manifest in the NMSSM where the rôle of Φ is played by the MSSM-like heavy doublet, but the argument is more general. In the present paper we have studied the prospects for corresponding searches in the $b\bar{b}b\bar{b}$, $b\bar{b}\tau\tau$ and $b\bar{b}\gamma\gamma$ final states, including SM backgrounds. We found that significant regions in the NMSSM parameter space can be tested by these searches:

The NMSSM specific parameters testable by $b\bar{b}b\bar{b}$ are typically in the region $\lambda \sim 0.50 - 0.70$ (the conservative upper bound from the absence of a Landau singularity below M_{GUT}), $\kappa \sim 0.4 - 0.7$, $\tan\beta \sim 2 - 3.5$, $\mu_{eff} \sim 180 \text{ GeV} - 290 \text{ GeV}$, $A_\lambda \sim 150 \text{ GeV} - 550 \text{ GeV}$, $A_\kappa \sim -830 \text{ GeV} - -210 \text{ GeV}$. An exception is the case $M_{H_S} \sim 85 \text{ GeV} - 110 \text{ GeV}$ where LEP constraints on the coupling of H_S to the Z boson are somewhat weaker; here values of λ down to 0.16 and μ down to 100 GeV (together with $\tan\beta$ up to 4.5) can lead to testable points. These ranges of potentially testable parameters depend little on the total integrated luminosity, but higher luminosity increases of course the number testable parameters within these ranges. Most of the parameters testable by $b\bar{b}\gamma\gamma$ are in the same region except for $\kappa \sim 0.08 - 0.3$, $A_\kappa \sim -50 \text{ GeV} - 10 \text{ GeV}$ which indicates that this region is non-overlapping

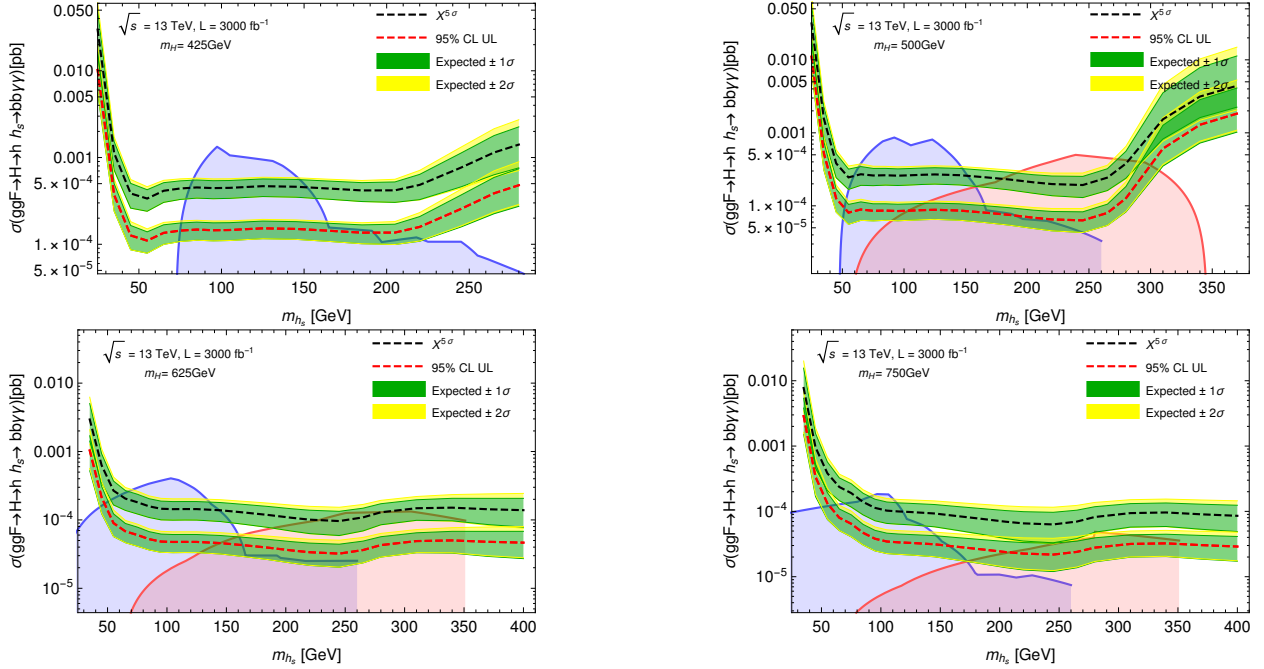


Figure 20: 95% CL exclusion limits and 5σ discovery cross sections for $H_{125} \rightarrow b\bar{b}$ and $H_S \rightarrow \gamma\gamma$ as function of M_{H_S} for 3000 fb^{-1} integrated luminosity and $M_H = 425$ GeV (upper left), $M_H = 500$ GeV (upper right), $M_H = 625$ GeV (lower left), $M_H = 750$ GeV (lower right). The colored regions are explained in the caption of Fig. 8.

with the one testable by $b\bar{b}b\bar{b}$.

We are convinced that the here proposed search methods can still be refined, and that the estimated sensitivities to cross sections times branching fractions presented here are conservative. This becomes clear from a comparison to the recent CMS search for resonant SM-Higgs pair production [21] in the $b\bar{b}\gamma\gamma$ final state (and actually also from a comparison to the recent CMS search [19] in the $b\bar{b}\tau\tau$ final state). Thus we hope that such promising searches will be performed in the future at the LHC.

Acknowledgements

This project has received support from the European Union’s Horizon 2020 research and innovation programs ITN HiggsTools (PITN-GA-2012-316704), ITN Elusives (Marie Skłodowska-Curie grant agreement No 674896), RISE InvisiblesPlus (Marie Skłodowska-Curie grant agreement No 690575), RISE NonMinimalHiggs (Marie Skłodowska-Curie grant agreement No 645722), the ERC advanced grant Higgs@LHC, and the Défi InPhyNiTi project N2P2M-SF. M.R.V. thanks Marius Wiesemann, Fady Bishara, Dirk E. Zerwas, Nikola Makovec, Sophie Henrot, Alberto Escalante and Davide Napoletano for fruitful discussions and help, and the hospitality received at the IPPP at the University of Durham, where part of this work has been done.

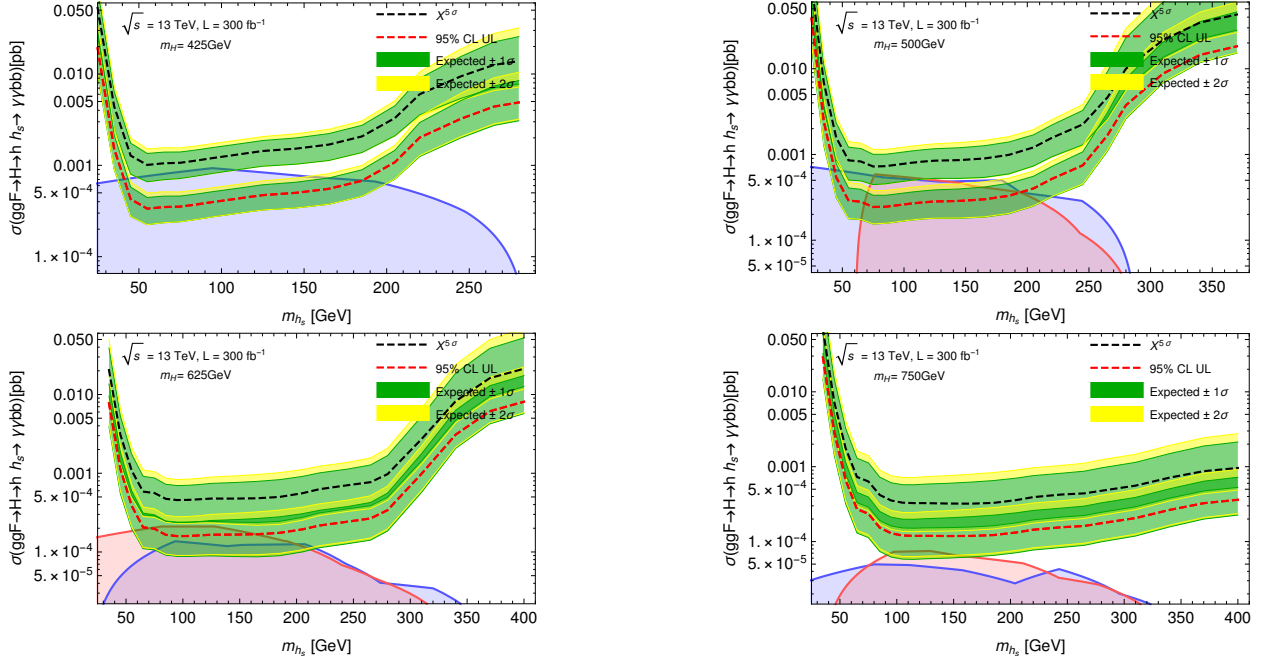


Figure 21: 95% CL exclusion limits and 5σ discovery cross sections for $H_{125} \rightarrow \gamma\gamma$ and $H_S \rightarrow b\bar{b}$ as function of M_{H_S} for 300 fb^{-1} integrated luminosity and $M_H = 425 \text{ GeV}$ (upper left), $M_H = 500 \text{ GeV}$ (upper right), $M_H = 625 \text{ GeV}$ (lower left), $M_H = 750 \text{ GeV}$ (lower right). The colored regions are explained in the caption of Fig. 8.

Appendix A: Functions to Fit Background Distributions

In this appendix we define the functions used to parametrize the total invariant mass (or M_X) distributions of the backgrounds to the various final states. The best choice among the functions and the values of the corresponding parameters have been obtained by maximum likelihood estimates.

Four Parameter Gamma distribution:

$$f(M_X; \alpha, \beta, \gamma, \mu) = \frac{\gamma}{\beta\Gamma(\alpha)} e^{-\left(\frac{M_X - \mu}{\beta}\right)^\gamma} \left(\frac{M_X - \mu}{\beta}\right)^{\alpha\gamma - 1} \quad \text{for } M_X \geq \mu, \\ f(M_X; \alpha, \beta, \gamma, \mu) = 0 \quad \text{for } M_X \leq \mu, \quad (\text{A.1})$$

Frechet distribution:

$$f(M_X; \alpha, \beta, \mu) = \frac{\alpha}{\beta} e^{-\left(\frac{M_X - \mu}{\beta}\right)^\alpha} \left(\frac{M_X - \mu}{\beta}\right)^{-\alpha - 1} \quad \text{for } M_X \geq \mu, \\ f(M_X; \alpha, \beta, \mu) = 0 \quad \text{for } M_X \leq \mu, \quad (\text{A.2})$$

GaussExp function:

A Gaussian with an exponential tail:

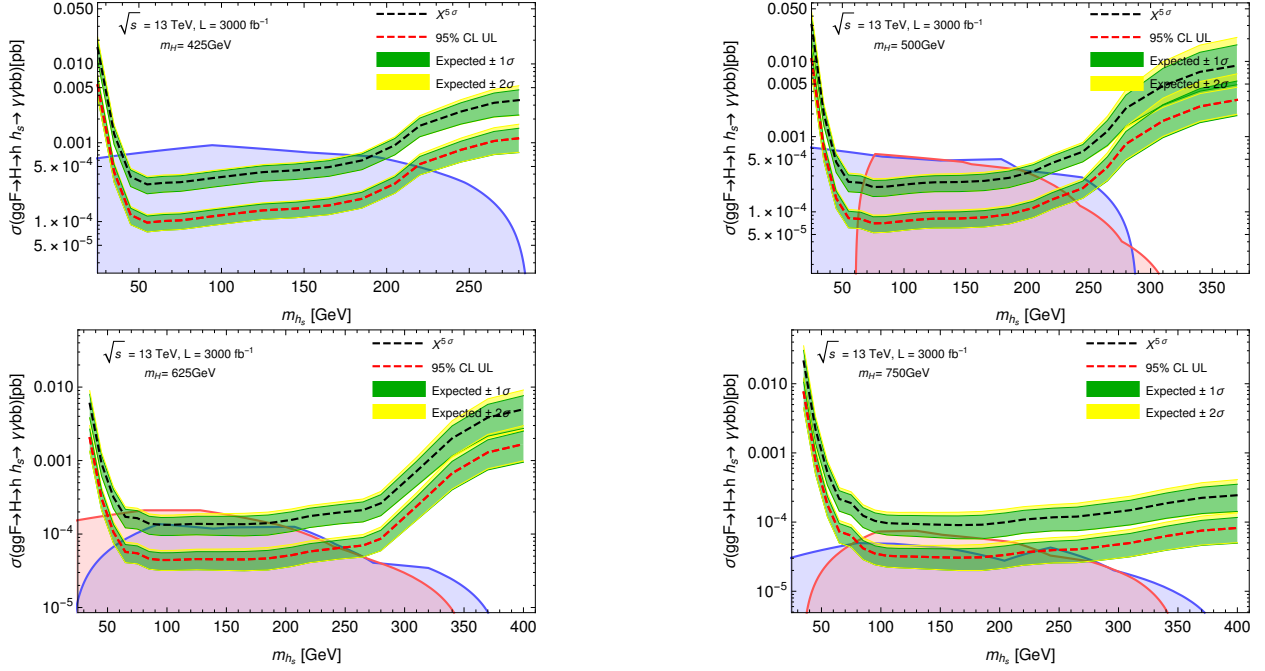


Figure 22: 95% CL exclusion limits and 5σ discovery cross sections for $H_{125} \rightarrow \gamma\gamma$ and $H_S \rightarrow b\bar{b}$ as function of M_{H_S} for 3000 fb^{-1} integrated luminosity and $M_H = 425 \text{ GeV}$ (upper left), $M_H = 500 \text{ GeV}$ (upper right), $M_H = 625 \text{ GeV}$ (lower left), $M_H = 750 \text{ GeV}$ (lower right). The colored regions are explained in the caption of Fig. 8.

$$\begin{aligned}
 f(M_X; \mu, \sigma, k) &= e^{-\frac{(M_X - \mu)^2}{2\sigma^2}} & \text{for } \frac{M_X - \mu}{\sigma} \leq k, \\
 f(M_X; \mu, \sigma, k) &= e^{\frac{k^2}{2} - \frac{k(M_X - \mu)}{\sigma}} & \text{for } \frac{M_X - \mu}{\sigma} > k.
 \end{aligned} \tag{A.3}$$

Landau Distribution

$$f(M_X; \mu, \sigma) = \int_0^\infty \sin(2t) e^{-t\left(\frac{M_X - \mu}{\sigma}\right) - \frac{2t}{\pi} \log(t)} dt \tag{A.4}$$

Appendix B: 5σ Discovery and 95% CL Exclusion Limits

In this appendix we sketch the computations of 5σ discovery and 95% CL exclusion limits based on the M_X distributions of the background, and the different M_X signal distributions (depending on M_{H_S}), following [53].

As shown in Fig. 4 the M_X distribution of the signal, after event selection and cuts, corresponds to a certain number s_i of expected signal events per bin. (The bin size in M_X is 20 GeV, and we have checked that the final results do not vary with this size.) From the MC simulation we know how this event number depends on the total signal cross section σ_{sig} ,

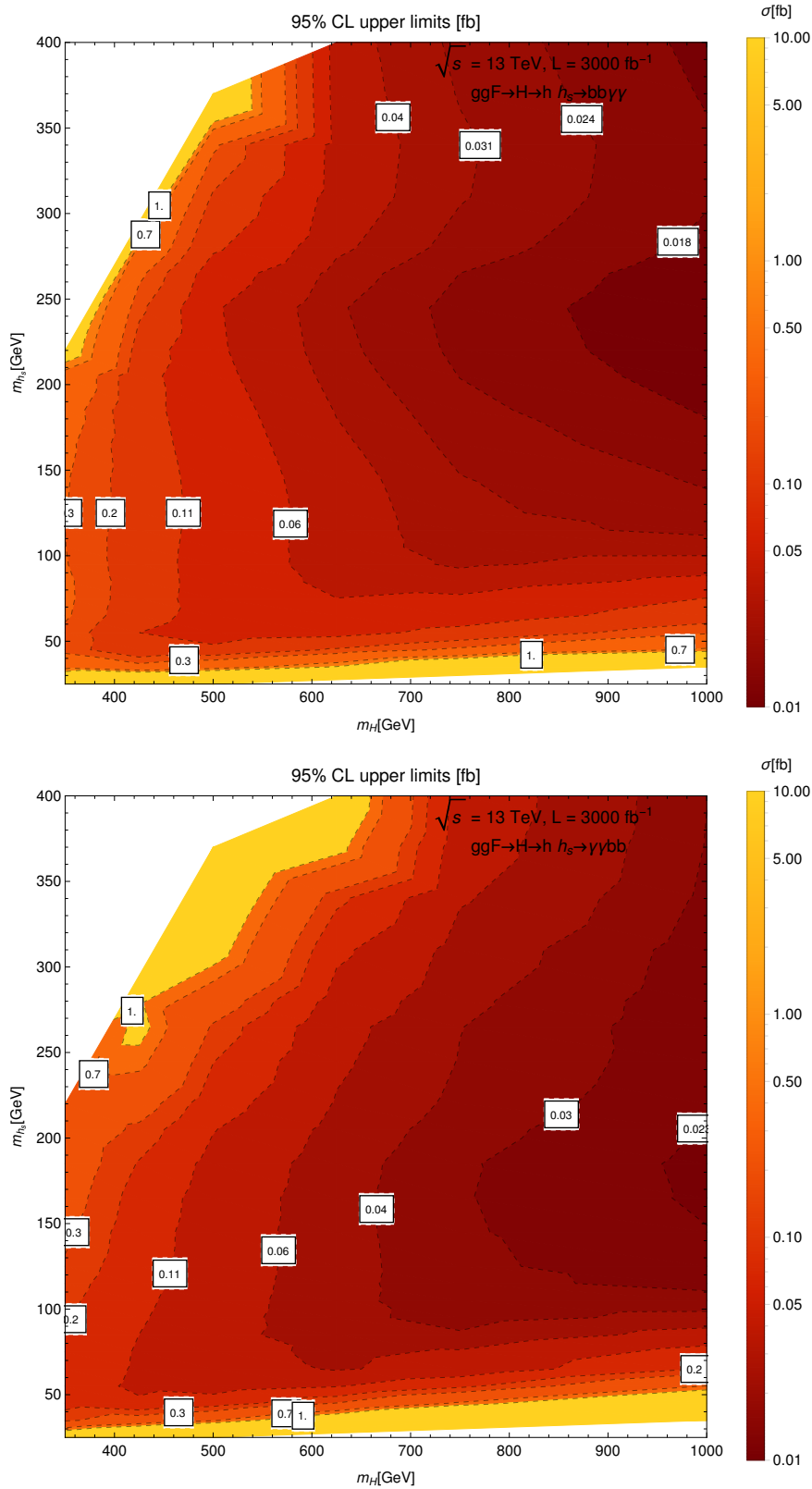


Figure 23: 95% CL expected upper limits for an integrated luminosity $L=3000\text{fb}^{-1}$ for the process $ggF \rightarrow H \rightarrow H_{125}(b\bar{b})H_S(\gamma\gamma)$ (up) and $ggF \rightarrow H \rightarrow H_{125}(\gamma\gamma)H_S(b\bar{b})$ (down), using m_X as the final discriminant.

the integrated luminosity \mathcal{L}_{int} and the acceptance A times efficiency ϵ :

$$s_i \sim \mathcal{L}_{int} \cdot \sigma_s \cdot \langle A \cdot \epsilon \rangle_s \quad (\text{B.1})$$

where \sim indicates a bin-dependent proportionality factor < 1 . The backgrounds after event selection and cuts have been fitted by continuous functions of $f(M_X)$ normalized to 1. Thus the number b_i of expected background events per bin per integrated luminosity is

$$b_i = \mathcal{L}_{int} \cdot \sigma_b \cdot \langle A \cdot \epsilon \rangle_b \cdot \int_{bin\ i} f(M_X) dM_X. \quad (\text{B.2})$$

Due to the large number of simulated events the statistical uncertainties around the median values $\langle A \cdot \epsilon \rangle_s$ and $\langle A \cdot \epsilon \rangle_b$ are negligibly small, $\lesssim 1\%$ in practically all cases.

Subsequently we use likelihood functions

$$L(\sigma_a, \sigma_b) = \prod_i \frac{(b_i + \sigma_a s_i)^{b_i + \sigma_b s_i}}{(b_i + \sigma_b s_i)!} e^{-(b_i + \sigma_a s_i)} \quad (\text{B.3})$$

with $(b_i + \sigma_b s_i)!$ interpolated by the Γ function for non integer $(b_i + \sigma_b s_i)$.

For 5σ discovery limits on σ_{sig} we look for the value of σ_{sig} for which the background only hypothesis is rejected at the 5σ level. The observed number of events per bin would be $b_i + \sigma_{sig} s_i$, and the likelihood function corresponding to the background only hypothesis is $L(0, \sigma_{sig})$. As function of the number of events per bin it has its maximum at $L(\sigma_{sig}, \sigma_{sig})$. Hence the test statistics t_{disc} for discovery is

$$t_{disc} = -2 \ln \frac{L(0, \sigma_{sig})}{L(\sigma_{sig}, \sigma_{sig})}. \quad (\text{B.4})$$

Following [53] the significance Z_{disc} is then

$$Z_{disc} = \sqrt{t_{disc}}, \quad (\text{B.5})$$

and for a 5σ discovery we determine σ_{sig} such that $Z_{disc} = 5$.

For 95% CL exclusion limits on σ_{sig} we look for the value of σ_{sig} for which the signal hypothesis is rejected at 95% CL. The observed number of events per bin would be b_i , and the likelihood function corresponding to the signal hypothesis is $L(\sigma_{sig}, 0)$. As function of the number of events per bin it has its maximum at $L(0, 0)$. Hence the test statistics t_{excl} for exclusion is

$$t_{excl} = -2 \ln \frac{L(\sigma_{sig}, 0)}{L(0, 0)}. \quad (\text{B.6})$$

For exclusion at 95% CL we determine σ_{sig} such that $\sqrt{t_{excl}} = 1.64$ since we consider only positive signal contributions to the number of events.

Uncertainties from the background are estimated as follows: $\pm(1 - 2)\sigma$ statistical uncertainties can be obtained bin by bin. To these we add linearly (to be conservative) the estimated $(1 - 2)\sigma$ systematic uncertainties from the overall normalisation of the background. Then the above likelihoods are recomputed with correspondingly larger and smaller values for all b_i from which we deduce the $\pm(1 - 2)\sigma$ uncertainties of σ_{sig} for the 5σ discovery limits and 95% CL exclusion limits.

References

- [1] [ATLAS Collaboration], “A search for resonant Higgs-pair production in the $b\bar{b}b\bar{b}$ final state in pp collisions at $\sqrt{s} = 8$ TeV”, ATL-CONF-2014-005
- [2] G. Aad *et al.* [ATLAS Collaboration], “Search For Higgs Boson Pair Production in the $\gamma\gamma b\bar{b}$ Final State using pp Collision Data at $\sqrt{s} = 8$ TeV from the ATLAS Detector,” Phys. Rev. Lett. **114** (2015) no.8, 081802 [arXiv:1406.5053 [hep-ex]].
- [3] G. Aad *et al.* [ATLAS Collaboration], “Search for Higgs boson pair production in the $b\bar{b}b\bar{b}$ final state from pp collisions at $\sqrt{s} = 8$ TeV with the ATLAS detector,” Eur. Phys. J. C **75** (2015) no.9, 412 [arXiv:1506.00285 [hep-ex]].
- [4] G. Aad *et al.* [ATLAS Collaboration], “Searches for Higgs boson pair production in the $hh \rightarrow bb\tau\tau, \gamma\gamma WW^*, \gamma\gamma bb, bbbb$ channels with the ATLAS detector,” Phys. Rev. D **92** (2015) 092004 [arXiv:1509.04670 [hep-ex]].
- [5] The ATLAS collaboration, “Search for Higgs boson pair production in the $b\bar{b}\gamma\gamma$ final state using pp collision data at $\sqrt{s} = 13$ TeV with the ATLAS detector,” ATLAS-CONF-2016-004.
- [6] [ATLAS Collaboration], “Search for pair production of Higgs bosons in the $b\bar{b}b\bar{b}$ final state using proton–proton collisions at $\sqrt{s} = 13$ TeV with the ATLAS detector ATL-CONF-2016-049
- [7] V. Khachatryan *et al.* [CMS Collaboration], “Search for two Higgs bosons in final states containing two photons and two bottom quarks in proton-proton collisions at 8 TeV,” Phys. Rev. D **94**, no. 5, 052012 (2016) [arXiv:1603.06896 [hep-ex]].
- [8] CMS Collaboration [CMS Collaboration], “Search for di-Higgs resonances decaying to 4 bottom quarks,” CMS-PAS-HIG-14-013.
- [9] V. Khachatryan *et al.* [CMS Collaboration], “Searches for heavy Higgs bosons in two-Higgs-doublet models and for $t \rightarrow ch$ decay using multilepton and diphoton final states in pp collisions at 8 TeV,” Phys. Rev. D **90** (2014) 112013 [arXiv:1410.2751 [hep-ex]].
- [10] V. Khachatryan *et al.* [CMS Collaboration], “Search for resonant pair production of Higgs bosons decaying to two bottom quark-antiquark pairs in proton-proton collisions at 8 TeV,” Phys. Lett. B **749** (2015) 560 [arXiv:1503.04114 [hep-ex]].
- [11] V. Khachatryan *et al.* [CMS Collaboration], “Searches for a heavy scalar boson H decaying to a pair of 125 GeV Higgs bosons hh or for a heavy pseudoscalar boson A decaying to Zh, in the final states with $h \rightarrow \tau\tau$,” Phys. Lett. B **755** (2016) 217 [arXiv:1510.01181 [hep-ex]].
- [12] V. Khachatryan *et al.* [CMS Collaboration], “Search for heavy resonances decaying to two Higgs bosons in final states containing four b quarks,” Eur. Phys. J. C **76** (2016) no.7, 371 [arXiv:1602.08762 [hep-ex]].

- [13] A. M. Sirunyan *et al.* [CMS Collaboration], “A search for Higgs boson pair production in the $b\bar{b}\tau\tau$ final state in proton-proton collisions at $\sqrt{s} = 8$ TeV,” arXiv:1707.00350 [hep-ex].
- [14] CMS Collaboration [CMS Collaboration], “Search for resonant pair production of Higgs bosons decaying to two bottom quark-antiquark pairs in proton-proton collisions at 13 TeV,” CMS-PAS-HIG-16-002.
- [15] CMS Collaboration [CMS Collaboration], “Search for heavy resonances decaying to a pair of Higgs bosons in four b quark final state in proton-proton collisions at $\sqrt{s} = 13$ TeV,” CMS-PAS-B2G-16-008.
- [16] CMS Collaboration [CMS Collaboration], “Search for resonant Higgs boson pair production in the $b\bar{b}\tau^+\tau^-$ final state,” CMS-PAS-HIG-16-013.
- [17] CMS Collaboration [CMS Collaboration], “Search for resonant Higgs boson pair production in the $b\bar{b}\tau^+\tau^-$ final state using 2016 data ,” CMS-PAS-HIG-16-029.
- [18] CMS Collaboration [CMS Collaboration], “Search for $H(b\bar{b})H(\gamma\gamma)$ decays at $\sqrt{s} = 13$ TeV,” CMS-PAS-HIG-16-032.
- [19] A. M. Sirunyan *et al.* [CMS Collaboration], “Search for Higgs boson pair production in events with two bottom quarks and two τ leptons in proton-proton collisions at $\sqrt{s} = 13$ TeV,” arXiv:1707.02909 [hep-ex].
- [20] CMS Collaboration [CMS Collaboration], “Search for resonant and non-resonant Higgs boson pair production in the $b\bar{b}l\nu l\nu$ final state at $\sqrt{s} = 13$ TeV,” CMS-PAS-HIG-17-006.
- [21] CMS Collaboration [CMS Collaboration], “Search for Higgs boson pair production in the final state containing two photons and two bottom quarks in proton-proton collisions at $\sqrt{s} = 13$ TeV,” CMS-PAS-HIG-17-008.
- [22] A. Djouadi, Phys. Rept. **459** (2008) 1 [hep-ph/0503173].
- [23] A. Djouadi and J. Quevillon, JHEP **1310**, 028 (2013) [arXiv:1304.1787 [hep-ph]].
- [24] A. Djouadi, L. Maiani, A. Polosa, J. Quevillon and V. Riquer, JHEP **1506** (2015) 168 [arXiv:1502.05653 [hep-ph]].
- [25] M. Maniatis, Int. J. Mod. Phys. A **25** (2010) 3505 [arXiv:0906.0777 [hep-ph]].
- [26] U. Ellwanger, C. Hugonie and A. M. Teixeira, Phys. Rept. **496** (2010) 1 [arXiv:0910.1785 [hep-ph]].
- [27] Z. Kang, J. Li, T. Li, D. Liu and J. Shu, Phys. Rev. D **88** (2013) no.1, 015006 [arXiv:1301.0453 [hep-ph]].
- [28] S. F. King, M. Mühlleitner, R. Nevzorov and K. Walz, Phys. Rev. D **90** (2014) no.9, 095014 [arXiv:1408.1120 [hep-ph]].

- [29] M. Carena, H. E. Haber, I. Low, N. R. Shah and C. E. M. Wagner, Phys. Rev. D **93** (2016) no.3, 035013 [arXiv:1510.09137 [hep-ph]].
- [30] U. Ellwanger and M. Rodriguez-Vazquez, JHEP **1602** (2016) 096 [arXiv:1512.04281 [hep-ph]].
- [31] R. Costa, M. Mühlleitner, M. O. P. Sampaio and R. Santos, JHEP **1606** (2016) 034 [arXiv:1512.05355 [hep-ph]].
- [32] S. Baum, K. Freese, N. R. Shah and B. Shakya, Phys. Rev. D **95** (2017) no.11, 115036 [arXiv:1703.07800 [hep-ph]].
- [33] S. von Buddenbrock *et al.*, Eur. Phys. J. C **76** (2016) no.10, 580 doi:10.1140/epjc/s10052-016-4435-8 [arXiv:1606.01674 [hep-ph]].
- [34] U. Ellwanger, J. F. Gunion and C. Hugonie, JHEP **0502** (2005) 066 [arXiv:hep-ph/0406215].
- [35] U. Ellwanger and C. Hugonie, Comput. Phys. Commun. **175** (2006) 290 [arXiv:hep-ph/0508022].
- [36] G. Degrossi and P. Slavich, Nucl. Phys. B **825** (2010) 119 [arXiv:0907.4682 [hep-ph]].
- [37] twiki.cern.ch/twiki/bin/view/LHCPhysics/CERNYellowReportPageBSMAt13TeV
- [38] J. Alwall *et al.*, JHEP **1407** (2014) 079 [arXiv:1405.0301 [hep-ph]].
- [39] R. V. Harlander, S. Liebler and H. Mantler, Comput. Phys. Commun. **184** (2013) 1605 [arXiv:1212.3249 [hep-ph]].
- [40] S. Liebler, Eur. Phys. J. C **75** (2015) no.5, 210 [arXiv:1502.07972 [hep-ph]].
- [41] H. Mantler and M. Wiesemann, Eur. Phys. J. C **75** (2015) no.6, 257 [arXiv:1504.06625 [hep-ph]].
- [42] R. D. Ball *et al.* [NNPDF Collaboration], Nucl. Phys. B **877** (2013) 290 [arXiv:1308.0598 [hep-ph]].
- [43] T. Sjostrand, S. Mrenna and P. Z. Skands, JHEP **0605** (2006) 026 [hep-ph/0603175].
- [44] J. de Favereau *et al.* [DELPHES 3 Collaboration], JHEP **1402** (2014) 057 [arXiv:1307.6346 [hep-ex]].
- [45] M. Cacciari and G. P. Salam, Phys. Lett. B **641** (2006) 57 [hep-ph/0512210].
- [46] ATLAS Collaboration, “Expected performance of the ATLAS b-tagging algorithms in Run-2”
- [47] M. Cacciari, M. Czakon, M. Mangano, A. Mitov and P. Nason, Phys. Lett. B **710** (2012) 612 [arXiv:1111.5869 [hep-ph]].

- [48] M. Czakon and A. Mitov, *Comput. Phys. Commun.* **185** (2014) 2930 [arXiv:1112.5675 [hep-ph]].
- [49] P. Baernreuther, M. Czakon and A. Mitov, *Phys. Rev. Lett.* **109** (2012) 132001 [arXiv:1204.5201 [hep-ph]].
- [50] M. Czakon and A. Mitov, *JHEP* **1212** (2012) 054 [arXiv:1207.0236 [hep-ph]].
- [51] M. Czakon and A. Mitov, *JHEP* **1301** (2013) 080 [arXiv:1210.6832 [hep-ph]].
- [52] M. Czakon, P. Fiedler and A. Mitov, *Phys. Rev. Lett.* **110** (2013) 252004 [arXiv:1303.6254 [hep-ph]].
- [53] G. Cowan, K. Cranmer, E. Gross and O. Vitells, *Eur. Phys. J. C* **71** (2011) 1554 Erratum: [*Eur. Phys. J. C* **73** (2013) 2501] [arXiv:1007.1727 [physics.data-an]].